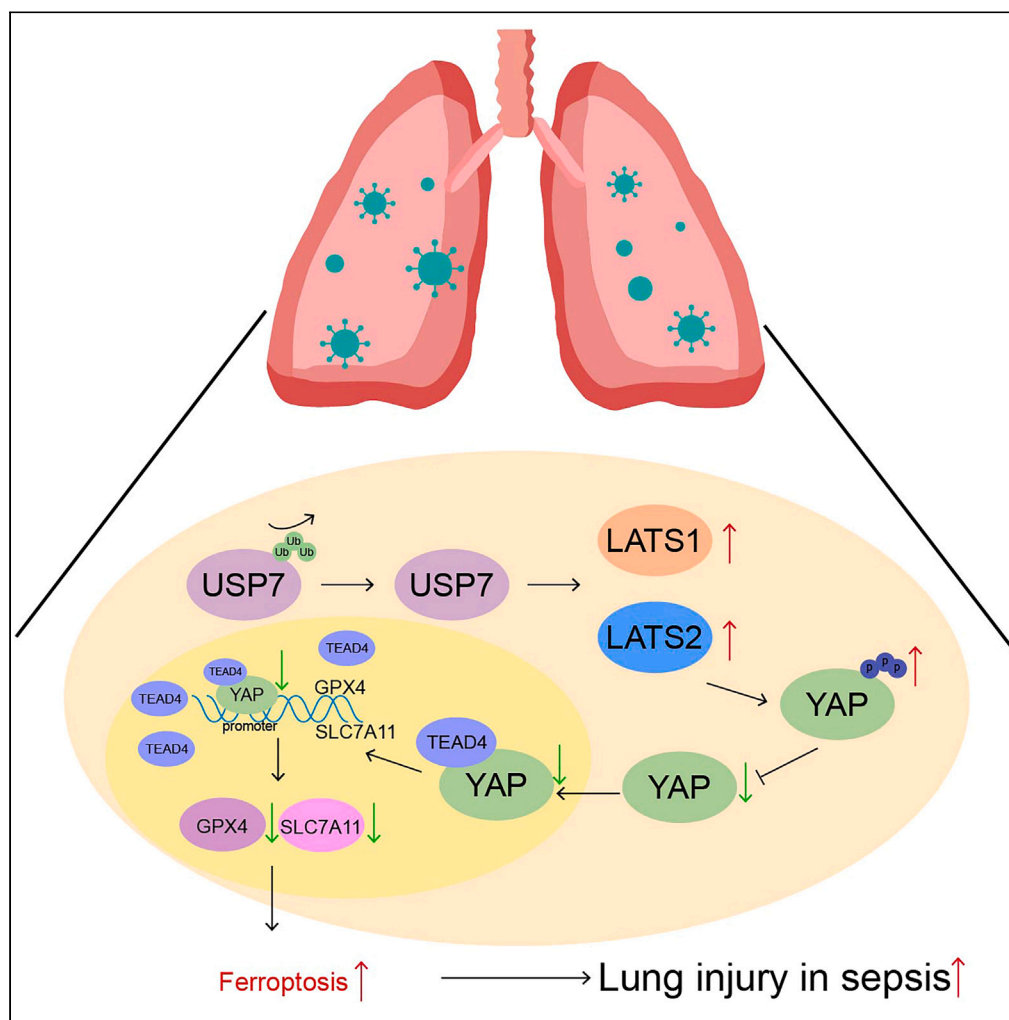# iScience

Article

USP7 upregulated by *TGF-β1* promotes ferroptosis via inhibiting *LATS1-YAP* axis in sepsis-induced acute lung injury

Hong Lv, Jing Yu, Xingjia Qian, ..., Guiqin Fan, Bufeng Zhuang, Bing Lu

zhuangbf2010@hotmail.com (B.Z.)
tczyylb@163.com (B.L.)

Highlights

TGF-β1 aggravated ferroptosis in both cellular and animal ALI models

USP7 downregulated YAP by deubiquitinating and stabilizing LATS1/2

YAP regulated the binding of TEAD4 to the promoters of GPX4 and SLC7A11

Ferroptosis was attenuated by YAP overexpression or silencing of USP7 or LATS1

Article

USP7 upregulated by *TGF-β1* promotes ferroptosis via inhibiting *LATS1-YAP* axis in sepsis-induced acute lung injury

Hong Lv,[1,4] Jing Yu,[1,4] Xingjia Qian,[1] Jun Shu,[1] Qiuhong Qian,[1] Luhong Shen,[1] Dongfang Shi,[1] Zhengzheng Tao,[1] Guiqin Fan,[1,2] Bufeng Zhuang,[3,*] and Bing Lu[1,5,*]

SUMMARY

Our work aimed to investigate the interactive roles of transforming growth factor β1 (TGF-β1), ubiquitin-specific-processing protease 7 (USP7), and Yes-associated protein (YAP) in ferroptosis during sepsis-secondary acute lung injury (ALI). Our study demonstrated that ferroptosis was aggravated by TGF-β1 in both cellular and animal models of acute lung injury. Additionally, YAP upregulated glutathione peroxidase 4 (GPX4) and SLC7A11 by regulating the binding of TEAD4 to GPX4/SLC7A11 promoters. Furthermore, large tumor suppressor kinase 1 (LATS1) knockdown resulted in YAP expression stimulation, while USP7 downregulated YAP via deubiquitinating and stabilizing LATS1/2. YAP overexpression or USP7/LATS1 silencing reduced ferroptosis process, which regulated YAP through a feedback loop. However, TGF-β1 annulled the repression of ferroptosis by YAP overexpression or LATS1/USP7 knockdown. By elucidating the molecular interactions between TGF-β1, USP7, LATS1/2, and YAP, we identified a new regulatory axis of ferroptosis in sepsis-secondary ALI. Our study sheds light on the pathophysiology of ferroptosis and proposes a potential therapeutic approach for sepsis-induced ALI.

INTRODUCTION

Sepsis may arise when the body's innate immune system malfunctions and reacts excessively to a bacterial or viral infection.[1] If sepsis worsens, it can cause complications such as kidney failure, organ death, and permanent lung damage. Sepsis-induced acute lung injury (ALI) is a perilous pulmonary inflammation that is typically marked by diffuse alveolar edema that can rapidly lead to fatal respiratory failure.[2] Worldwide, 20% of people die from sepsis,[3] with sepsis-induced ALI being the leading cause of sepsis-related deaths.[4] Despite considerable efforts and numerous clinical interventions aimed at improving patient outcomes over the past few decades, sepsis and its secondary ALI remain critical health issues due to their poor prognosis.[5]

Ferroptosis is a newly discovered regulated cell death process that differs from apoptosis and autophagy, and is characterized by iron-driven lipid peroxidation. When the metabolism of cellular reactive oxygen species (ROS) is out of homeostatic balance and excess lipid peroxides accumulate to a lethal level, ferroptotic cell death is triggered.[6] The acyl-CoA synthetase long-chain family member 4 (ACSL4) plays an essential role in the execution of ferroptosis among the enzymes that regulate fatty acid mentalism. The removal of ACSL4 led to a significant reduction in ferroptosis among acute kidney injury mice.[7] It was recently reported that ferroptosis is present during progression of ALI induced by intestinal ischemia reperfusion (IIR)[8] or lipopolysaccharide (LPS).[9] It is noteworthy that both aforementioned studies demonstrated that treatment with ferrostatin-1 (Fer-1), the ferroptosis inhibitor, significantly ameliorated LPS- or IIR-induced ALI in cellular and animal models. However, the precise physiological role of ferroptosis in the pathogenesis of ALI pathogenesis is still obscure and has not yet been investigated or reported.

The Hippo-pathway effector YAP (Yes-associated protein) functions as the phosphorylation substrate of large tumor suppressor kinase (LATS) 1/2 and has become a prominent determinant of ferroptosis.[10] Following nuclear translocation, the N-terminal domain of YAP forms a structural complex with the C-terminal domain of the nuclear constitutive TEA domain transcription factor (TEAD4).[11] TEAD4 acquires its full transcriptional activity, regulating both cell proliferation and survival.[12] It has been discovered that in hepatocellular carcinoma, YAP boosts SLC7A11 expression by binding with TAZ to the ATF4 transcription factor, granting resistance to sorafenib-induced ferroptosis through a TEAD-dependent mechanism.[13] Conversely, YAP promotes ferroptosis by upregulating SKP2 in multiple cancer cell lines.[14] It has been

[1]Department of Pulmonary and Critical Care Medicine, Taicang TCM Hospital, Affliated to Nanjing University of Chinese Medicine, Taicang, Jiangsu Province 215499, P.R. China
[2]Soochow University School of Medicine, Suzhou, Jiangsu Province 215031, P.R. China
[3]Department of Thoracic Surgery, Shanghai Ninth People's Hospital, Shanghai Jiaotong University School of Medicine, Shanghai 200011, P.R. China
[4]These authors contributed equally
[5]Lead contact
*Correspondence: zhuangbf2010@hotmail.com (B.Z.), tczyylb@163.com (B.L.)

reported that the activation of Hippo-YAP can protect against endotoxemic ALI.[15] However, it remains unknown whether and how YAP is involved in the ferroptosis during sepsis-induced ALI progression.

Glutathione peroxidase 4 (GPX4) is crucial in maintaining lipid homeostasis and degrading toxic lipid hydroperoxides, utilizing reduced glutathione (GSH) as electron donors.[16] GPX4 deactivation causes the abnormal accumulation of lipid peroxides, resulting in ferroptotic cell death in cardiomyocytes,[17] cancer,[18] and IIR-induced ALI.[8] Another crucial regulator of ferroptosis is the cystine/glutamate antiporter SLC7A11. Cellular deficiency of SLC7A11 drives ferroptosis by blocking cysteine uptake and GSH biosynthesis is eventually inhibited.[19] Consequently, SLC7A11/GPX4 axis is considered as an effective ferroptosis-suppressing mechanism. In this investigation, we performed bioinformatic analysis of JASPAR database and identified potential binding sites between the promoters of GPX4/SLC7A11 and TEAD4. We hypothesized that the expression of GPX4 and SLC7A11 could be modulated by TEAD4. On the other hand, we computed that LATS1 underwent deubiquitination by the ubiquitin-specific-processing protease 7 (USP7), and we anticipated that stabilization of LATS1 consequently resulted in the degradation of YAP. Su et al. previously showed that elevated USP7 expression in ALI mice exacerbated inflammatory responses via stabilization of Tip60.[20] Intriguingly, USP7 was shown to accelerate ferroptosis in the rat heart and kidney after ischemia/reperfusion.[21,22] Transforming growth factor β1 (TGF-β1) is a pleiotropic cytokine that regulates cell growth, differentiation, and immune responses. Excessive TGF-β1 activity has been reported to contribute to the development of pulmonary fibrosis in ALI.[23] However, its direct connection to ferroptosis in ALI has not been extensively investigated. No investigation or observation has been made on the crosstalk among TGF-β1, USP7, LATS1, YAP, and SLC7A11/GPX4 axis regarding ferroptosis in ALI.

The present study utilized bioinformatics methods and *in vitro* and *in vivo* experimental assays to investigate the regulatory mechanism of TGF-β1-USP7-YAP-GPX4/SLC7A11 in ferroptosis during the occurrence and progression of sepsis-secondary ALI. Our work identified that USP7 was regulated by TGF-β1 and mediated YAP degradation, which led to GPX4/SLC7A11 downregulation and exacerbated ferroptosis in an ALI model induced by LPS or cecal ligation and puncture (CLP). These outcomes offer potential for advancing the discovery of innovative treatment for sepsis-caused ALI.

RESULTS

TGF-β1 aggravated lung damage symptoms in septic animal model and increased ferroptosis-induced mouse mortality

TGF-β1 is a cytokine with anti-inflammatory properties, although its overexpression has been observed in patients with sepsis-induced lung injury.[24] However, its clinical significance is multifaceted and an excessive TGF-β1 activity can contribute to exacerbated lung damage by stimulating ROS-induced stress.[25] To explore the pathological and physiological roles of TGF-β1 in sepsis-induced ALI, we have established a septic mouse model by performing CLP procedures. A mouse survival curve was then produced using the Kaplan-Meier approach. As illustrated in Figure 1A, the survival rate of mice significantly decreased upon CLP operation in comparison to the sham group. Nevertheless, the CLP-shortened life span was efficiently rescued by Fer-1 treatment (CLP + Fer-1), which inhibited ferroptosis process in the mice. Mice subjected to CLP along with administration of iron (CLP + Fe) or TGF-β1-treatment (CLP + TGF-β1) demonstrated the lowest survival rates among all experimental groups, indicating that TGF-β1 exacerbates ferroptosis. The rescue effect of Fer-1 was also observed in the CLP+TGF-β1+Fer-1 group. Our findings indicate that survival rate was increased in the CLP+TGF-β1+Fer-1 group compared to the CLP + TGF-β1 group. Consistent with our findings on survival rates, H&E staining revealed marked pulmonary injury in mice subjected to CLP compared to sham-operated mice (Figure 1B). Mice treated with TGF-β1 underwent the most severe lung injury, with injury scores only marginally lower than those in the CLP + Fe group (Figure 1C). The CLP+TGF-β1+Fer-1 group exhibited lower lung injury than the CLP + TGF-β1 group (Figure 1C). We also estimated the lung water accumulation by calculating the wet/dry lung ratio. CLP-operated mice obtained a significantly higher wet/dry lung ratio than the sham group, suggesting that ferroptosis-related excess pulmonary extravascular liquid was elevated by CLP operation (Figure 1D). Both the CLP + Fe and CLP + TGF-β1 groups exhibited the highest wet/dry lung ratios. However, the CLP+TGF-β1+Fer-1 group showed a decreased value compared to the CLP + TGF-β1 group (Figure 1D). Accumulation of lipid peroxide end-product malondialdehyde (MDA) is directly correlated with ferroptosis sensitivity. In contrast, GSH shields cells from ferroptosis by reducing ROS. Additionally, depletion of GSH was shown to trigger cellular ferroptosis.[26] Thus, we next evaluated the MDA and GSH levels in animal lung tissue pulp samples. Indeed, we observed a significant increase in MDA level within the lung tissue of mice undergoing CLP surgery compared to the sham group. Moreover, MDA levels were more elevated in the CLP-mice who received TGF-β1, but decreased in the CLP+TGF-β1+Fer-1 group (Figure 1E). Conversely, we recorded significantly reduced GSH levels in the lung tissue of the CLP-mice, in comparison to the sham group (Figure 1F). This decrease in GSH depletion aligns with erastin inducing cell death through oxidative stress, following ROS production stimulation.[18] CLP and TGF-β1 treatment resulted in similar GSH levels in lung tissue as the CLP + Fe group, but levels increased in the CLP+TGF-β1+Fer-1 group. Lipid ROS content among specific groups was then measured (Figure 1G). Both the CLP + Fe and CLP + TGF-β1 groups demonstrated the higher lipid ROS content, compared with CLP group. However, the decreased lipid ROS in CLP+TGF-β1+Fer-1 group was shown compared to the CLP + TGF-β1 group (Figure 1G). To understand the molecular mechanisms underlying the TGF-β1-induced ferroptosis, we examined the protein expression of USP7, LATS1/2, YAP, SLC7A11, GPX4, and ACSL4 in mouse lung tissue samples. As illustrated by our western blot analysis results, we detected significantly lower molecular levels of YAP, SLC7A11, and GPX4 in mice that underwent CLP surgery compared to sham-operated mice (Figure 1H). Fer-1 treatment rescued protein expression, but it was considerably reduced in both CLP + TGF-β1 and CLP + Fe groups. Notably, the CLP+TGF-β1+Fer-1 group showed lower expression than the CLP + TGF-β1 group. In contrast, the expression of USP7, LATS1, LATS2, and ACSL4 was increased by the CLP operation and Fe and TGF-β1 treatment, but decreased with Fer-1 administration (Figure 1H). These data aforementioned firstly confirmed that we have efficiently
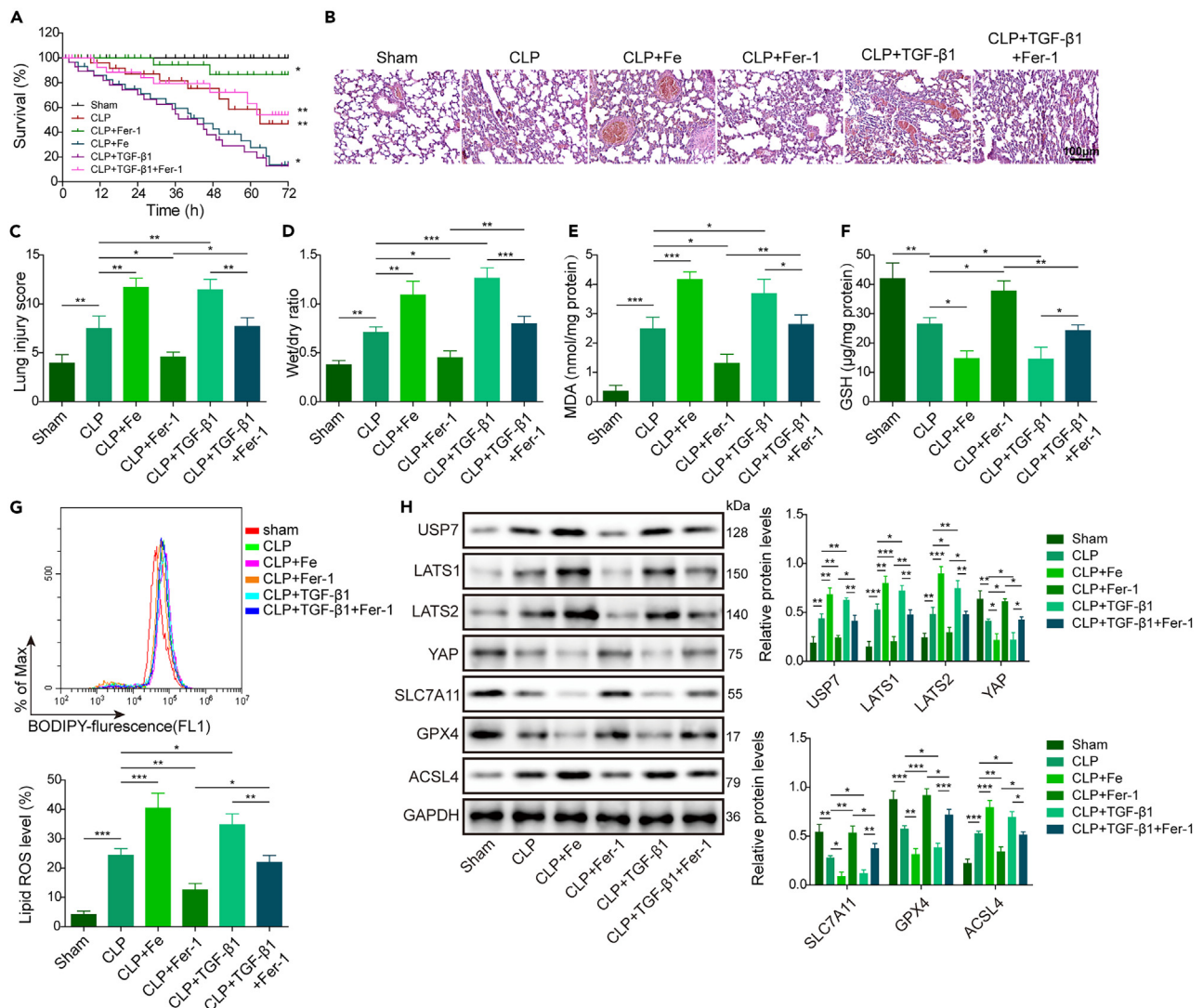
Figure 1. TGF-β1 aggravated the lung damage symptoms in septic mice and increased ferroptosis-induced mouse mortality

Acute lung injury was induced by performing acute lung injury operation.

(A) Survival rate of CLP mice, CLP group treated with Fe, Ferrostatin-1 (Fer-1), or TGF-β1 and the sham-operated control group were observed every 12 h after CLP or sham surgery.

(B) Mouse lung samples were collected and histopathological changes were examined by H&E staining (Scale bar, 100 μm).

(C) Lung injury scores were compared among sham group, CLP group, and CLP group treated with Fe, Fer-1, or TGF-β1.

(D) Mouse lung weight was measured and the wet-to-dry ratio was calculated in each group.

(E) The lipid peroxide MDA and (F) GSH expression levels were detected by in each group.

(G) Lipid ROS content was detected in each group.

(H) Western blot analysis was performed to evaluate the expression of USP7, LATS1/2, YAP, GPX4, SLC7A11, and ACSL4. Data were presented as mean ± standard deviation (S.D). $N = 6$, $*p < 0.05$, $**p < 0.01$, $***p < 0.001$ by one-way ANOVA test for A, C–H.

established an animal model with sepsis-induced ALI symptoms. Additionally, our findings presented the primary *in vivo* empirical substantiation that TGF-β1 escalates sepsis-induced lung injuries and aggravated ferroptosis in mice.

TGF-β1 promoted *in vitro* ferroptosis in LPS plus erastin-induced septic cells

We next employed an LPS plus erastin-induced cellular sepsis model to further examine the function of TGF-β1 during ferroptosis. Erastin, a cell-permeable ferroptosis activator, induces cellular lipid ROS accumulation by regulating ACSL4.[27] To establish an *in vitro* septic model, MLE-12 cells were stimulated with LPS (5 μg/mL) for 24 h (Figure S1), and further MTT assay results indicate that cell death was triggered by gradually increasing concentrations of erastin, while the mortality rate of LPS-treated cells was considerably higher than that of the control
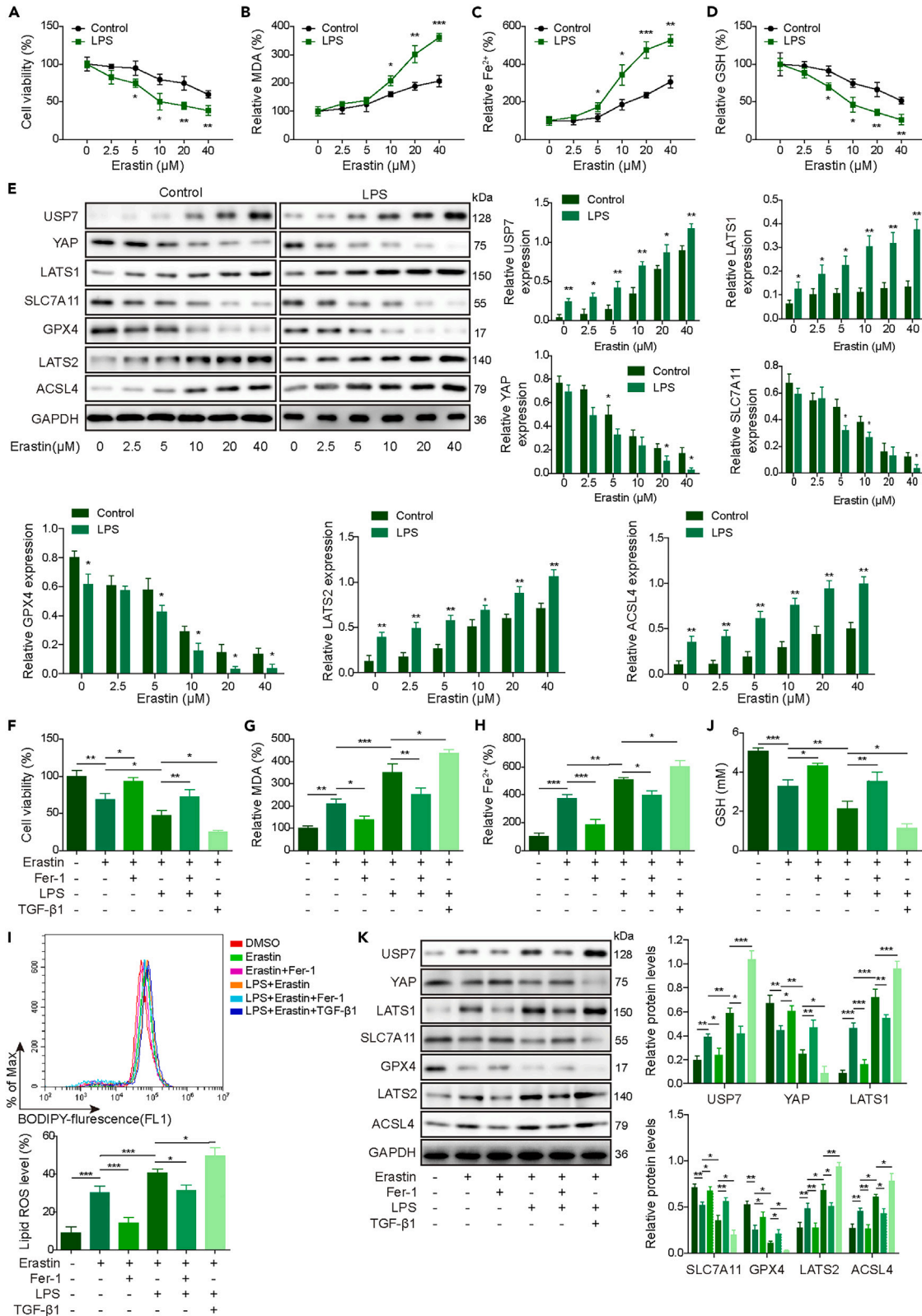
Figure 2. TGF-β1 promoted ferroptosis in cellular sepsis model

In vitro septic model was generated by stimulating the MLE-12 cells using LPS for 24 h when increasing concentration of erastin was added.

(A) Cell vitality was assessed by MTT assay.

(B) The lipid peroxide MDA expression level was compared between LPS-treated cells and the control.

(C) Cellular Fe^{2+} and (D) GSH change was measured.

(E) Protein expression levels of USP7, LATS1/2, YAP, GPX4, SLC7A11, and ACSL4 in LPS-treated cells and the control were detected by western blot.

(F) Cells were treated with LPS + Erastin + Fer-1, Erastin + Fer-1, LPS + Erastin + TGF-β1, Erastin + LPS, or Erastin alone and cellular death was examined by MTT assay.

(G) The lipid peroxide MDA expression level, (H) cellular Fe^{2+}, (I) lipid ROS content, and (J) GSH changes were compared among the groups above.

(K) Western blot analysis was conducted to detect the expression of USP7, LATS1/2, YAP, GPX4, SLC7A11, and ACSL4. The experiment was repeated independently at least three times, and data were presented as mean ± standard deviation (S.D).*$p < 0.05$, **$p < 0.01$, ***$p < 0.001$ by Student's t test for A–E, and by one-way ANOVA test for F–K.

group (Figure 2A). Subsequently, we compared the cellular MDA and Fe^{2+} levels after specific treatments. We detected significantly elevated MDA and Fe^{2+} concentrations in the LPS-stimulated MLE-12 cells compared to control cells (Figures 2B and 2C). In contrast, GSH level was decreased by LPS treatment when the cellular erastin concentration was increased (Figure 2D). This finding is consistent with the results of a previous study.[18] Additionally, we examined the protein expression of USP7, LATS1/2, YAP, SLC7A11, GPX4, and ACSL4 in MLE-12 cells. Our western blot results indicate that protein expression of YAP, SLC7A11, and GPX4 is markedly reduced in LPS-stimulated cells when compared to control cells (Figure 2E). In contrast, LPS led to an upregulation of USP7, LATS1/2, and ACSL4 expression. These data indicate the successful establishment of an *in vitro* sepsis model, whereby ferroptosis in MLE-12 cells was exacerbated upon LPS treatment and the increased concentration of erastin.

In order to explore the molecular function of TGF-β1 in our *in vitro* sepsis model, we supplemented LPS plus erastin-stimulated cells with recombinant TGF-β1, reaching a final concentration of 5 ng/mL. As illustrated by the MTT assay results, the addition of Fer-1 largely mitigated erastin-induced ferroptosis, whereas it was heightened under LPS stimulation (Figure 2F). We observed the highest death rate in the MLE-12 cells treated with LPS, erastin, and TGF-β1 (LPS + erastin + TGF-β1 group). In consistence with the MTT assay results, the upregulation effect of erastin on cellular MDA (Figure 2G), Fe^{2+} levels (Figure 2H), and lipid ROS (Figure 2I) was enhanced by LPS treatment but almost completely eliminated by Fer-1. Interestingly, we detected significantly higher MDA, Fe^{2+} concentrations, and lipid ROS in MLE-12 cells treated with erastin, LPS, and TGF-β1, than in those treated with only erastin and LPS. However, the LPS + erastin + TGF-β1 cell group exhibited an extremely low GSH level compared to all the other five groups of cells (Figure 2J). Additionally, we profiled USP7, LATS1/2, YAP, GPX4, SLC7A11, and ACSL4 expression. As shown in our western blot results, the expression of YAP, SLC7A11, and GPX4 was decreased by erastin and further diminished by LPS treatment. The protein expression was partially restored through Fer-1 intervention but entirely abolished among the cells subjected to LPS, erastin, and TGF-β1 (Figure 2K). In contrast, the expression of USP7, LATS1/2, and ACSL4 increased following erastin and LPS treatment. The highest USP7, LATS1/2, and ACSL4 expression was observed in LPS + erastin + TGF-β1 cells. Our results affirm the establishment of *in vitro* sepsis model and further manifest the promotional effect of TGF-β1 on ferroptosis progression in MLE-12 cells challenged with LPS plus erastin.

YAP overexpression upregulated GPX4 and attenuated cellular ferroptosis, while TGF-β1 suppressed YAP expression and antagonized YAP-induced ferroptosis-inhibition

To investigate the molecular mechanism underlying the inhibitory effect of TGF-β1 on ferroptosis, we first transfected MLE-12 cells with recombinant pcDNA3.1 vector carrying YAP gene and verified transfection efficiency by detecting YAP expression through western blot (Figure 3A). SLC7A11 and GPX4 expression was largely enhanced in the YAP-transfected MLE-12 cells. Then, we transfected the YAP-encoding pcDNA3.1 vectors into LPS-challenged MLE-12 cells. Our MTT assay results highlighted that YAP overexpression significantly enhanced viability in both LPS-challenged cells and those treated with LPS and TGF-β1 (Figure 3B) compared to the control groups. In accordance with our MTT results, the levels of MDA (Figure 3C) and Fe^{2+} (Figure 3D) as the indicative of ferroptosis, which were upregulated by LPS alone and further enhanced by LPS in combination with TGF-β1, were markedly reduced upon YAP overexpression. Conversely, the GSH level in cells treated with LPS or LPS plus TGF-β1 was rescued by YAP transfection (Figure 3E). We observed that cells treated with LPS and YAP had lower lipid ROS levels compared to those treated by LPS and empty vectors. Furthermore, the group treated with LPS+TGF-β1+YAP showed a significantly decreased lipid ROS level compared to the LPS+TGF-β1 and LPS+TGF-β1+empty vector groups (Figure 3F). In addition, we compared the protein expression of YAP, GPX4, SLC7A11, and ACSL4 in different cells (Figure 3G). Compared to the control cells, the expression of YAP, GPX4, and SLC7A11 was significantly decreased in LPS-stimulated cells, and this effect was further eliminated upon TGF-β1 treatment. However, the inhibitory effect of LPS and TGF-β1 on the expression of YAP, SLC7A11, and GPX4 was counteracted by YAP overexpression. However, the ACSL4 level was upregulated in LPS-stimulated cells and further enhanced by TGF-β1 treatment, which could be resisted by YAP overexpression (Figure 3G). Our findings are consistent with a prior investigation, which demonstrated a negative reciprocal regulation between YAP and ferroptosis in gastrointestinal cancer cell lines.[28] These presented results suggest that TGF-β1 promoted ferroptosis progression by inhibiting YAP, whose overexpression attenuated LPS-induced ferroptosis through upregulating SLC7A11 and GPX4.

LATS1 knockdown inhibited ferroptosis, and TGF-β1 hindered LATS1-knockdown-induced ferroptosis inhibition

We tested our hypothesis that TGF-β1 induces ferroptosis through its effects on YAP by transfecting MLE-12 cells with si-LATS1 for silencing. Western blot analysis revealed enhanced protein levels of YAP, GPX4, and SLC7A11, while LATS1 and ACSL4 were reduced upon LATS1
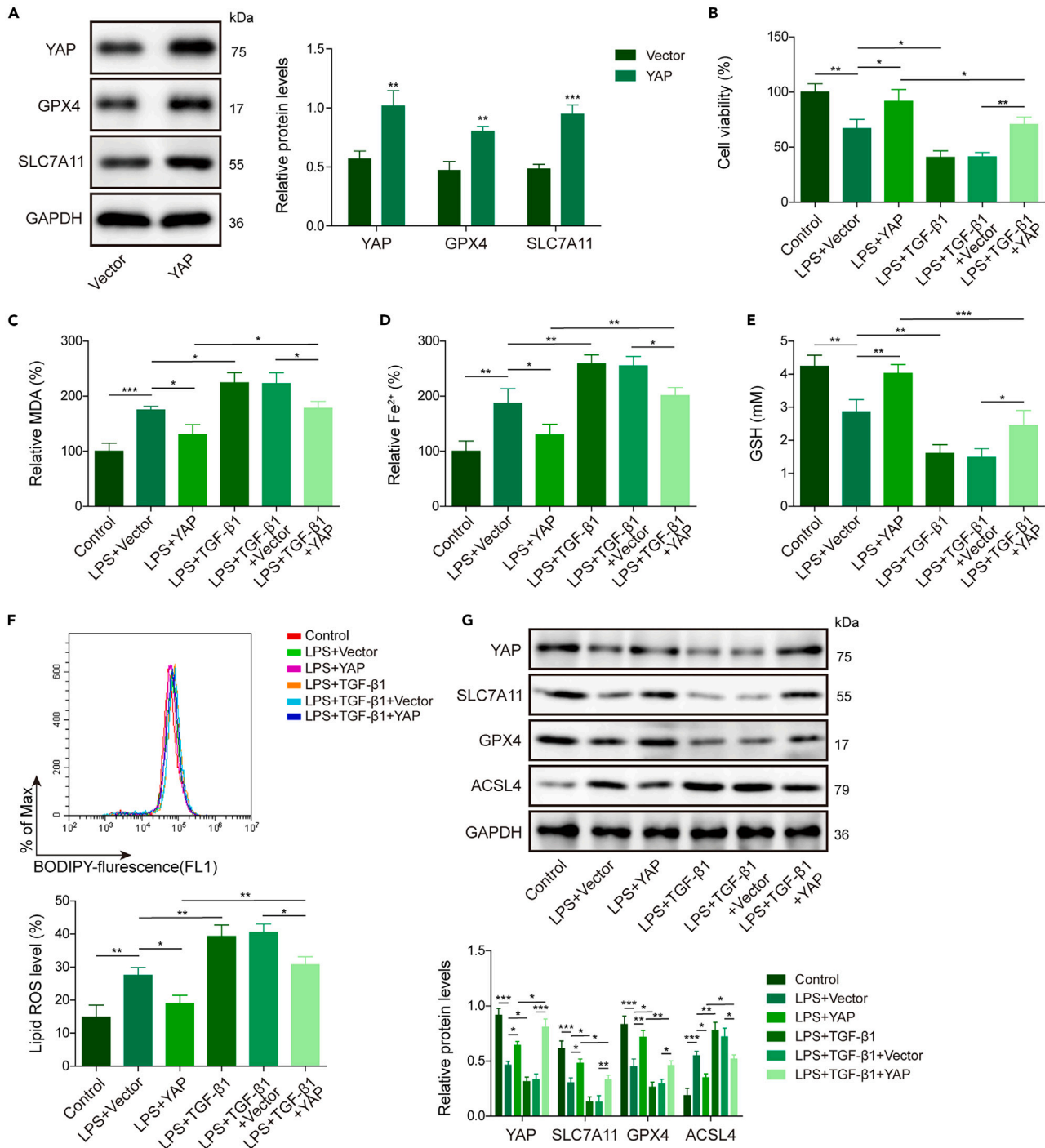
Figure 3. Overexpression of YAP enhanced GPX4/SLC7A11 expression in LPS-stimulated cells and inhibited *in vitro* ferroptosis, while the inhibitory effect was counteracted by TGF-β1 treatment

MLE-12 cells were treated with LPS for 24 h, followed by pcDNA3.1-YAP transfection (YAP).

(A) Expression changes of YAP, GPX4, and SLC7A11 upon YAP overexpression were examined by western blot analysis.

(B) MTT assay was conducted to evaluate the cell vitality in the indicated groups.

(C) The lipid peroxide MDA expression level was compared among the cells treated with LPS alone, LPS+ YAP, LPS + TGF-β1, LPS + TGF-β1 + Vector, or LPS + TGF-β1 + YAP transfection.

CellPress
OPEN ACCESS

knockdown (Figure 4A). Through our MTT assay, we noticed that the suppression of LATS1 effectively restored cellular viability which was decreased by LPS and further impaired by TGF-β1 (Figure 4B). In accord with our MTT results, MDA (Figure 4C) and Fe^{2+} (Figure 4D) concentrations were largely reduced after LATS1 silencing. By contrast, GSH concentration in cells treated by LPS or LPS plus TGF-β1 was rescued by LATS1 knockdown (Figure 4E). We observed decreased levels of lipid ROS in cells treated with LPS and si-LATS1 than in those treated with LPS and empty vectors. Furthermore, the group of cells treated with LPS+TGF-β1 + si-LATS1 showed significantly reduced levels of lipid ROS than the LPS+TGF-β1+si-NC group (Figure 4F). Meanwhile, we measured expression changes of LATS1, YAP, GPX4, SLC7A11, and ACSL4 under the specific conditions (Figure 4G). Compared to the control cells, LATS1 and ACSL4 expression increased in LPS-challenged cells whereas the expression of YAP, GPX4, and SLC7A11 decreased. Adding TGF-β1 intensified the effects. In contrast, LATS1 knockdown enhanced protein expression of YAP, GPX4, and SLC7A11, decreased the ACSL4 level, nullified the inhibition of LPS and TGF-β1 on YAP, GPX4, and SLC7A11, and abrogated the promotion effect of LPS and TGF-β1 on ACSL4. These results suggest that LATS1 knockdown inhibits ferroptosis through upregulation of GPX4 and SLC7A11 and downregulation of ACSL4; however, the effects were reversed by TGF-β1.

### USP7 knockdown promoted YAP-mediated ferroptosis suppression, while TGF-β1 upregulated USP7 and stimulated USP7-induced ferroptosis

Our bioinformatics (ubibrowser_v3, http://ubibrowser.bio-it.cn/ubibrowser_v3/) analysis showed that LATS1/2 was deubiquitinated by the USP7 and predicted that USP7 could stabilize LATS1/2 (Figure 5A). We investigated whether USP7onis involved in TGF-β1 induced ferroptosis from the perspective of LATS1/2 stability by transfecting MLE-12 cells with USP7-specific siRNA for knockdown. Western blot analysis showed that USP7 expression was efficiently silenced by si-USP7 (Figure 5B). Additionally, USP7 knockdown notably upregulated the expression levels of YAP, GPX4, and SLC7A11. However, LATS1/2 and ACSL4 expression were inhibited (Figure 5B). We next employed MTT assay to assess the cell viability. As illustrated in Figure 5C, USP7 knockdown effectively reduced cell death rates in LPS-challenged cells as well as in those treated with LPS and TGF-β1 (Figure 5C). MDA (Figure 5D) and Fe^{2+} (Figure 5E) levels, which serve as the indicative of ferroptosis, were found to be elevated in LPS-challenged cells and further promoted by TGF-β1, and were concordantly decreased when USP7 was silenced. On the other hand, USP7 knockdown effectively restored levels of GSH, which were reduced by LPS and TGF-β1 treatment (Figure 5F). Next, we detected lower lipid ROS levels in cells treated with LPS and si-USP7 than in those treated by LPS and empty vectors. Furthermore, cells treated with LPS+TGF-β1 + si-USP7 showed lower levels of lipid ROS than the LPS+TGF-β1+si-NC group (Figure 5G). We further analyzed the changes in expression of USP7, LATS1/2, YAP, GPX4, SLC7A11, and ACSL4 under the specified conditions (Figure 5H). Compared to the control group, the expression of YAP, SLC7A11, and GPX4 was downregulated in LPS-challenged cells which were further reduced by TGF-β1. The inhibitory effect was counteracted by si-USP7 transfection. By contrast, we observed enhanced expression of USP7, LATS1/2, and ACSL4 in LPS and TGF-β1-challenged MLE-12 cells, which was effectively inhibited following si-USP7 transfection (Figure 5H). These results collectively demonstrate that TGF-β1 upregulates USP7, whose knockdown mitigates the progression of ferroptosis.

YAP facilitated the expression of GPX4/SLC7A11 through its regulation of the association between their promoters and TEAD4

In order to scrutinize the connection between YAP and SLC7A11, as well as GPX4, we transfected MLE-12 cells with si-YAP to induce knockdown and gauged the expression of SLC7A11 and GPX4 by conducting a western blot. The protein levels of YAP, SLC7A11, and GPX4 were significantly suppressed after the si-YAP transfection (Figure 6A). Next, we accessed JASPAR database and calculated the binding profiles between TEAD4 and GPX4. The predicted sequences of TEAD4 that bind to the GPX4 promoter are AGGCTCTGTCCA (BS1, from −1880 to −1869) and CTGAGTCAC (BS2, from −1264 to −1256), as depicted in Figure 6B. The luciferase activity of GPX4 was dose dependently enhanced after transfection with YAP-overexpressed plasmids (Figure 6C). Notably, the increase in luciferase activity of GPX4 caused by YAP-mediated overexpression was nullified by the mutation of both BS1 and BS2, but not affected by the mutation of BS1 or BS2 alone (Figure 6D). The interactions were further experimentally investigated with chromatin immunoprecipitation (ChIP) assay (Figure 6E), indicating that YAP promotes TEAD4 binding to BS1 and BS2 of GPX4 promoter. Subsequently, we established *in vitro* sepsis-induced ALI model by stimulating MLE-12 cells with LPS. The luciferase reporter assay detected a decreased association between TEAD4 and the GPX4 promoter (Figure 6F). However, YAP overexpression largely rescued the binding of TEAD4 on the GPX4 promoter in LPS-treated cells.

We also computed the binding profiles between TEAD4 and SLC7A11. It was predicted that the TEAD4 binding sequences targeting the SLC7A11 promoter were CAGATAAGG (BS1, from −1612 to −1604) and AGAGTAAACA (BS2, from −1068 to −1259), as depicted in Figure 6G. Additionally, the luciferase activity of SLC7A11 was enhanced in a dose-dependent manner following transfection with YAP-overexpressed plasmids (Figure 6H). Moreover, when MLE-12 cells were transfected with YAP-expressing pcDNA 3.1 vector, luciferase activity of both SLC7A11-WT and the constructs carrying BS1 mutation significantly increased. However, the luciferase activity of SLC7A11-MUT2 carrying BS2 mutation alone, and the SLC7A11-MUT1&2 construct carrying both BS1 and BS2 mutations remained the same in the cells
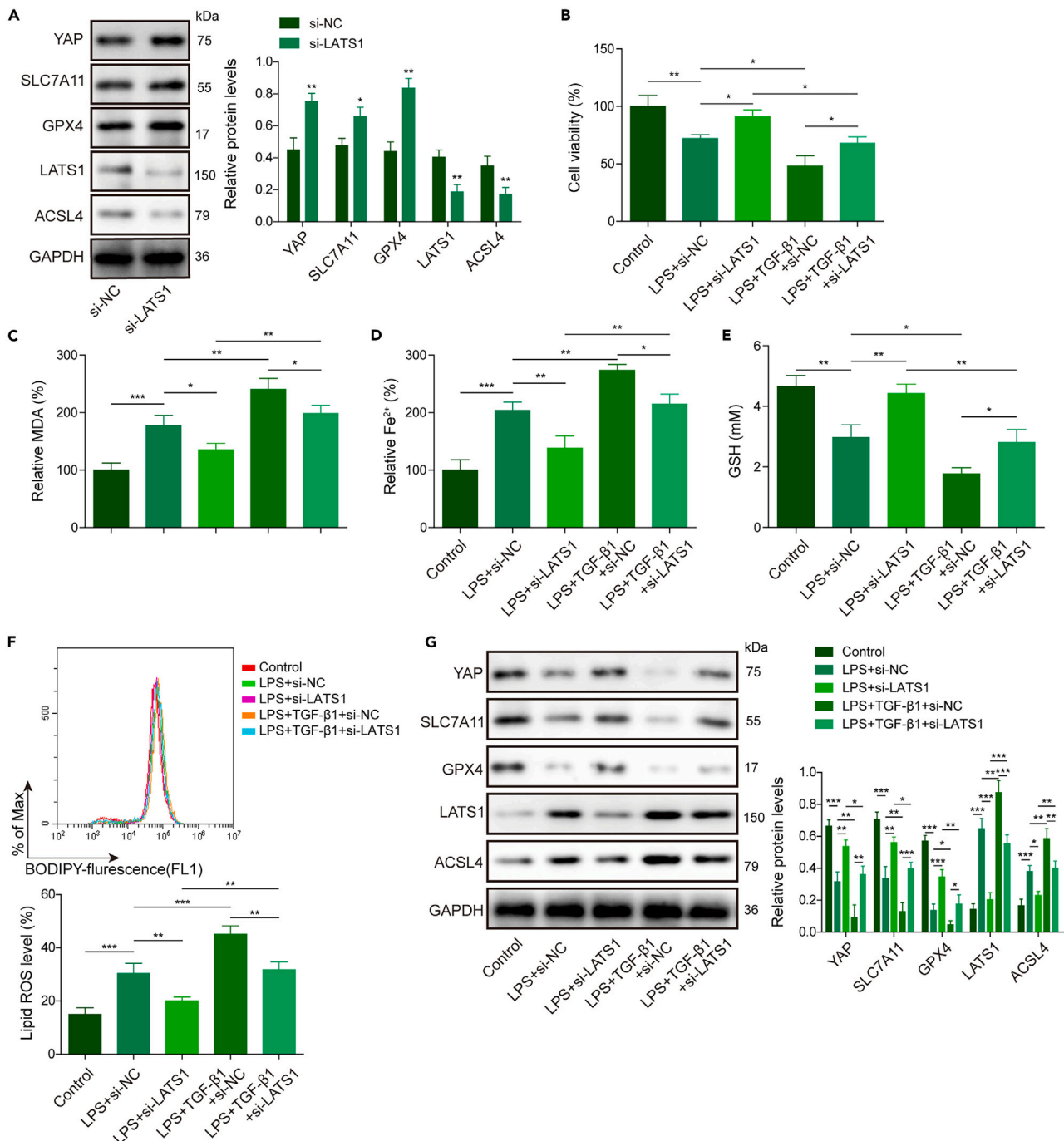
Figure 4. LATS1 knockdown upregulated GPX4 and SLC7A11 via YAP and repressed *in vitro* ferroptosis

MLE-12 cells were treated with LPS for 24 h, followed by si-LATS1 transfection.

(A) Protein expression of LATS1, YAP, GPX4, SLC7A11, and ACSL4 upon LATS1 knockdown was examined by western blot analysis.

(B) MTT assay was performed to evaluate the cell vitality in the MLE-12 cells which were treated with LPS alone, LPS + si-LATS1, LPS + TGF-β1, or LPS + TGF-β1 + si-LATS1.

(C) Indicated cells were treated with 10 μM erastin for 24 h and the lipid peroxide MDA expression level was compared among the indicated cells above.

(D) Cellular Fe^{2+} and (E) GSH changes were detected upon the specific treatments.

(F) Lipid ROS content was assessed in cellular models.

(G) Protein expression of LATS1, YAP, GPX4, SLC7A11, and ACSL4 in the cells above were measured by western blot analysis. The experiment was repeated independently at least three times, and data were presented as mean ± standard deviation (S.D).*$p < 0.05$, **$p < 0.01$, ***$p < 0.001$ by Student's t test for A, and by one-way ANOVA test for B–G.
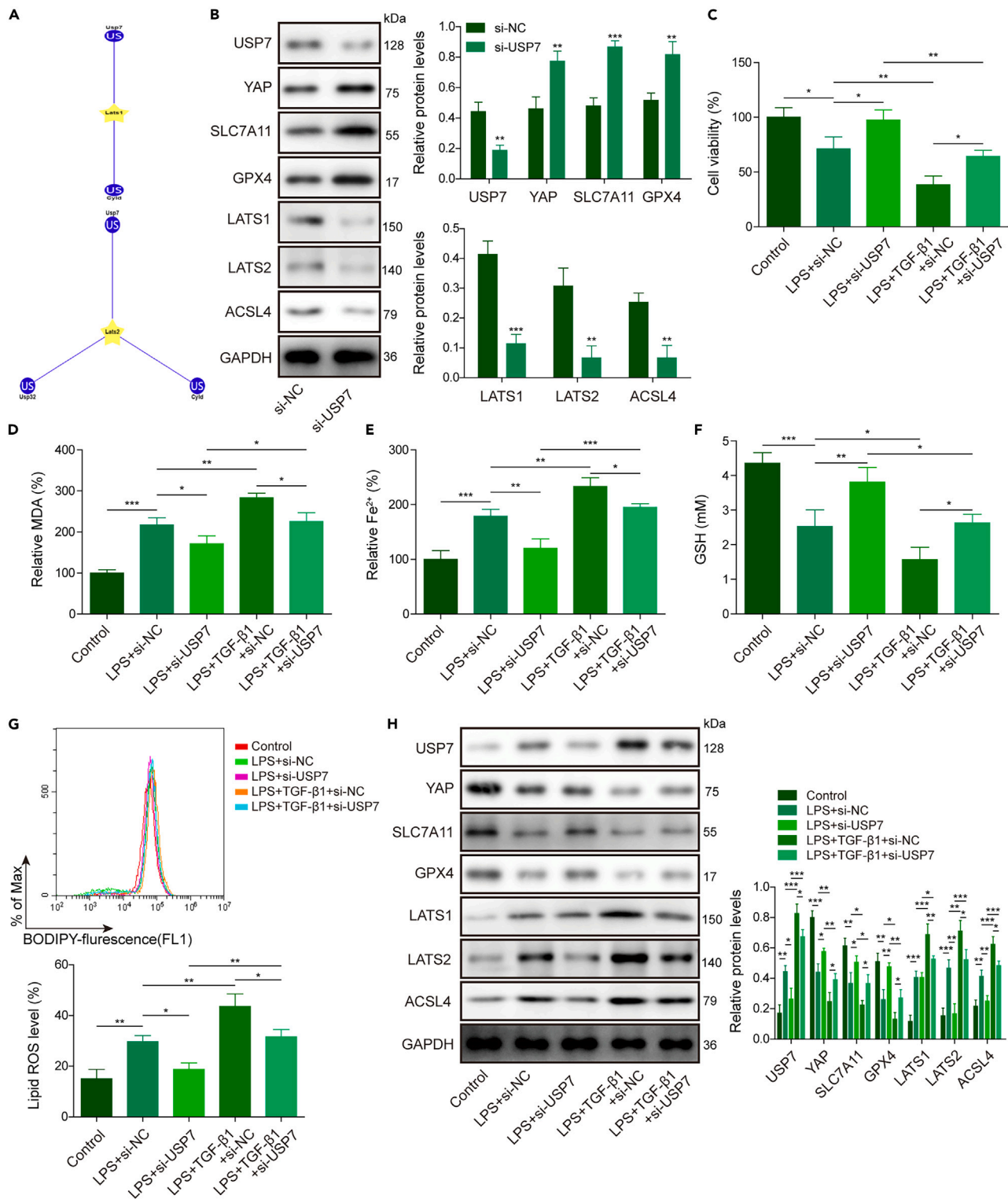
Figure 5. USP7 knockdown stimulated YAP expression and repressed *in vitro* ferroptosis

(A) LATS1/2 was deubiquitinated by USP7 through Ubibrowser database.

(B) MLE-12 cells were transfected with si-USP7 or si-NC, and protein expression of USP7, LATS1/2, YAP, GPX4, SLC7A11, and ACSL4 was analyzed by western blot.

(C) LPS-treated MLE-12 cells were transfected with si-USP7, si-NC, TGF-β1+ si-NC, or TGF-β1+ si-USP7, and cell vitality was assessed by MTT assay.

Figure 5. *Continued*

(D) The lipid peroxide MDA expression level was compared among the indicated cells above.

(E) Cellular Fe^{2+} and (F) GSH changes were measured upon the specific treatments.

(G) Lipid ROS content was detected in cellular models.

(H) Protein expression of USP7, LATS1/2, YAP, GPX4, SLC7A11, and ACSL44 in the cells above were detected by western blot analysis. The experiment was repeated independently at least three times, and data were presented as mean ± standard deviation (S.D.).*$p < 0.05$, **$p < 0.01$, ***$p < 0.001$ by Student's t test for B, and by one-way ANOVA test for B–H.

transfected with oe-YAP or an empty vector (Figure 6I). This was further illustrated in ChIP results (Figure 6J), indicating that YAP promotes TEAD4 binding to BS2 of the SLC7A11 promoter. Moreover, we performed luciferase reporter assay and detected a decreased association between TEAD4 and SLC7A11 promoter in our *in vitro* sepsis-induced ALI model, while MLE-12 cells were stimulated with LPS (Figure 6K). Nonetheless, YAP overexpression successfully reinstated the interaction between TEAD4 and the SLC7A11 promoter in LPS-treated cells.

Combining bioinformatics computational approaches with *in vitro* assays, we identified the specific intermolecular interaction between TEAD4 and GPX4/SLC7A11 promoters. YAP upregulated expression of GPX4 and SLC7A11 by modulating the association between TEAD4 and GPX4/SLC7A11 promoters.

USP7 degraded YAP by deubiquitinating and stabilizing LATS1

We performed co-immunoprecipitation pull-down assay and evaluated the physiological interaction between USP7 and LATS1 by using LATS1- and USP7-specific antibodies. Based on the findings presented in Figure 7A, we identified an entire LATS1-USP7 complex. Following this, we exposed USP7-silenced MLE-12 cells to MG132 and found that LATS1 expression repressed by si-USP7 was largely rescued by MG132 (Figure 7B). We then introduced CHX to the MLE-12 cells with USP7 knockdown and monitored changes in USP7, YAP, and LATS1 expression. Western blot assay showed that USP7-knockdown attenuated YAP degradation process, which was induced by CHX treatment, and accelerated LATS1 degradation rate (Figure 7C). Furthermore, we demonstrated that the ubiquitination process was accelerated following USP7 knockdown (Figure 7D). In addition, cellular death rate was assayed using the MTT method under the specific conditions. USP7 knockdown significantly restored the impaired cell viability by LPS stimulation, while this rescuing effect was prevented by YAP silencing (Figure 7E). In accord with the MTT results aforementioned, concentrations of the ferroptosis indicators MDA (Figure 7F) and Fe^{2+} (Figure 7G), which were elevated in LPS-challenged cells, were significantly downregulated when USP7 was silenced. In contrast, the concentration of GSH was restored upon USP7 knockdown (Figure 7H). The positive effects of USP7 knockdown were reversed when si-YAP was used to silence YAP expression. We observed an increase in lipid ROS levels in cells treated with LPS+si-USP7+si-YAP compared to those treated by LPS+si-USP7 (Figure 7I). Moreover, we found that the cellular expression of YAP, GPX4, and SLC7A11, which was decreased by LPS treatment, experienced recovery upon USP7 knockdown but largely eliminated after YAP expression was silenced (Figure 7J). However, USP7, LATS1/2, and ACSL4 expression, which had been enhanced by LPS, was reduced by USP7 knockdown and remained unaffected by simultaneous silencing of YAP. These results indicate that TGF-β1 suppresses YAP-mediated inhibition of ferroptosis by regulating USP7 directly. This is achieved through its role in stabilizing LATS1/2 and degrading YAP.

DISCUSSION

Patients with sepsis-related ALI are at high risk of mortality.[29] Ferroptosis, a newly discovered necrosis mechanism was initially defined in cancer cells as part of key tumor suppressor pathways.[30] Recently, Liu et al.[9] and Dong et al.[8] independently observed ferroptotic cell death in IIR- and LPS-induced ALI. TGF-β1 is recognized as a critical mediator of pulmonary edema in ALI.[23] It has been recently reported to be implicated in ferroptosis in hepatocellular carcinoma cells,[31] radiation-induced lung fibrosis,[32] as well as in diabetes-induced tubular injury.[33] However, the specific role of TGF-β1 in ferroptosis in ALI has not yet been reported. The present study identifies TGF-β1 as a ferroptosis inducer in both *in vitro* and *in vivo* ALI models. We also showed that although YAP expression was diminished by ferroptosis, overexpressing YAP or silencing USP7 or LATS1 safeguarded cells from ferroptosis by stimulating cellular expression of GPX4 and SLC7A11. However, treatment with TGF-β1 reversed the protective effect. Our current study highlights that targeting the TGF-β1/USP7/LATS1/YAP axis could be considered for treating sepsis-induced ALI. Dysregulated accumulation of inflammatory cytokines such as IL-6 and TGF-β1 has been identified as a key player in the pathogenesis of ALI.[34] For instance, Qian et al. showed that the downregulation of the anti-inflammatory factor TGF-β1 in ALI mice subjected to CLP led to augmented inflammation processes.[35] Recently, Kim et al. proposed that TGF-β1 sensitized hepatocellular carcinoma cells to a GPX4 inhibitor, promoting ferroptosis by activating ROS generation.[31] It is unclear whether and how TGF-β1 plays a role in the development of ferroptosis during ALI progression. To investigate this, we generated a peritoneal, polymicrobial septic murine model using CLP method as well as a cellular ALI model through LPS stimulation, followed by characterizing the hallmark features of ferroptosis. Upon analysis, we made a significant finding that TGF-β1 treatment exacerbates ALI symptoms in a mouse sepsis model and induces ferroptosis in both *in vitro* and *in vivo* ALI models. Our results indicate that TGF-β1 promotes ferroptotic cell death in the pathogenesis of sepsis-induced ALI. Further research is necessary to confirm these findings through clinical experiments.

The transcriptional coactivator YAP interacts with TEAD4 in the nucleus and functions as a key regulator of antioxidant responses. Suppression of YAP is commonly observed in cancer cells. Cellular expression of YAP is negatively regulated by LATS1.[36] Our bioinformatics analysis proposes USP7 as a stabilizer and deubiquitinating agent for LATS1/2. Although USP7 was previously reported to stabilize the transcriptional coactivators Yorkie[37] and TAZ,[38] we demonstrated in the presented study that USP7 functioned as a negative regulator of YAP since it
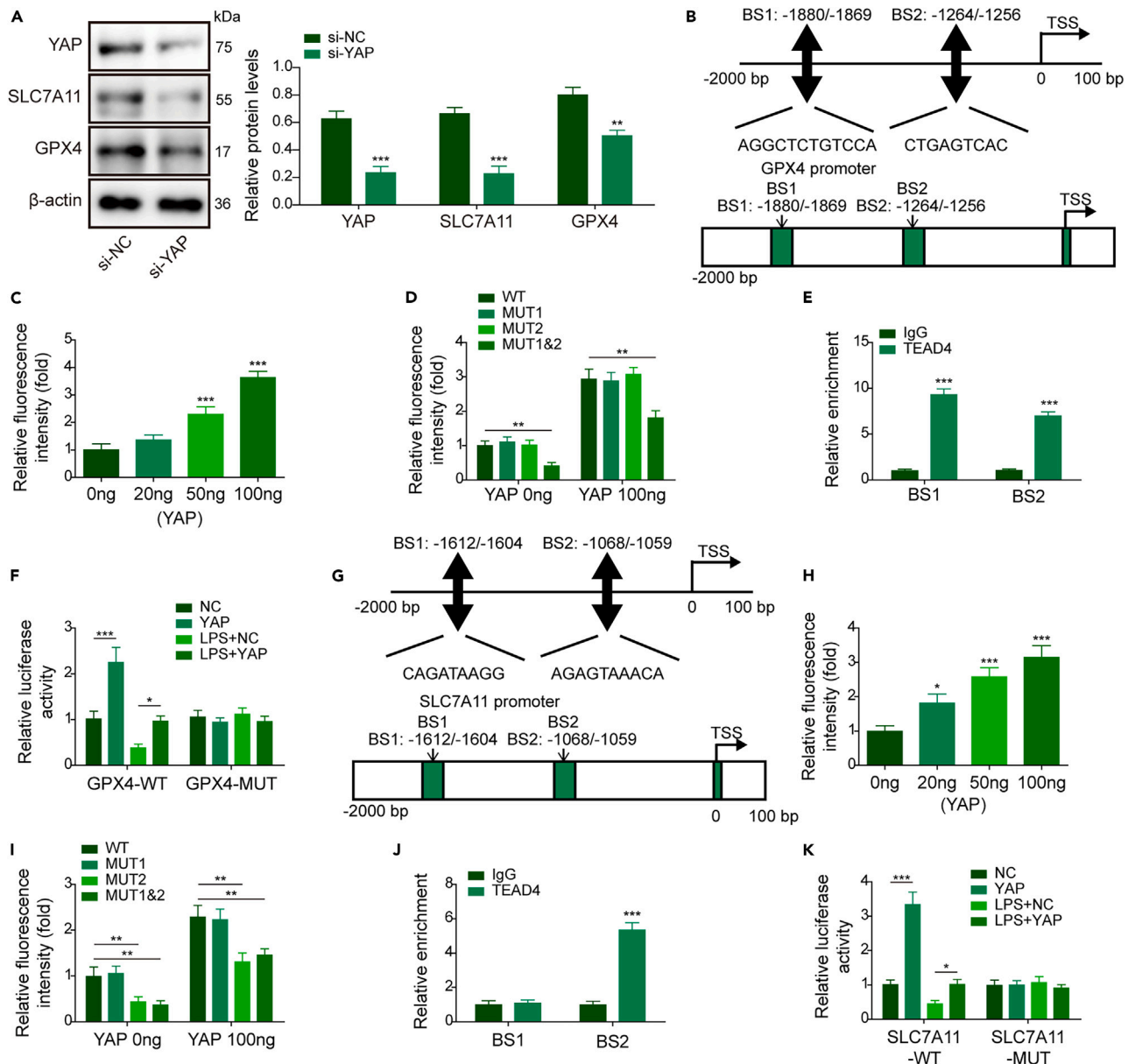
Figure 6. YAP modulates the binding between TEAD4 and GPX4/SLC7A11 promoter and promotes GPX4/SLC7A11 expression

(A) MLE-12 cells were transfected with si-NC or si-YAP, and protein expression of YAP, GPX4, and SLC7A11 was detected by western blot analysis.

(B) JASPAR was accessed and the computed binding sites between TEAD4 and GPX4 were shown.

(C) MLE-12 cells were transfected with 0, 20, 50, or 100 ng of YAP-overexpression plasmid vector. Dual-luciferase reporter assay was used to analyze the relative enrichment of TEAD4 at GPX4 promoter.

(D) Cells were transfected with 0 or 100 ng YAP and luciferase reporter assay was used to detect the intermolecular binding between TEAD4 and GPX4.

(E) The direct interaction between TEAD4 and GPX4 was further substantiated by ChIP assay.

(F) *In vitro* sepsis-induced ALI model was generated by stimulating MLE-12 cells with LPS. Molecular binding between TEAD4 and GPX4 was evaluated by luciferase reporter assay when YAP was overexpressed.

(G) JASPAR was accessed and the computed binding sites between TEAD4 and SLC7A11 were shown.

(H) MLE-12 cells were transfected with 0, 20, 50, or 100 ng of YAP-overexpression plasmid vector. Dual-luciferase reporter assay was used to analyze the relative enrichment of TEAD4 at SLC7A11 promoter.

(I) Cells were transfected with 0 or 100 ng YAP and luciferase reporter assay was used to detect the intermolecular binding between TEAD4 and SLC7A11.

(J) The direct interaction between TEAD4 and SLC7A11 was further substantiated by ChIP assay.

(K) YAP was overexpressed in MLE-12 cells induced with LPS. Luciferase reporter assay was performed to evaluate the molecular bindings between TEAD4 and SLC7A11. The experiment was repeated independently at least three times, and data were presented as mean ± standard deviation (S.D).*$p < 0.05$, **$p < 0.01$, ***$p < 0.001$ by Student's t test for A, E, J, and by one-way ANOVA test for C, D, F, H, I, K.
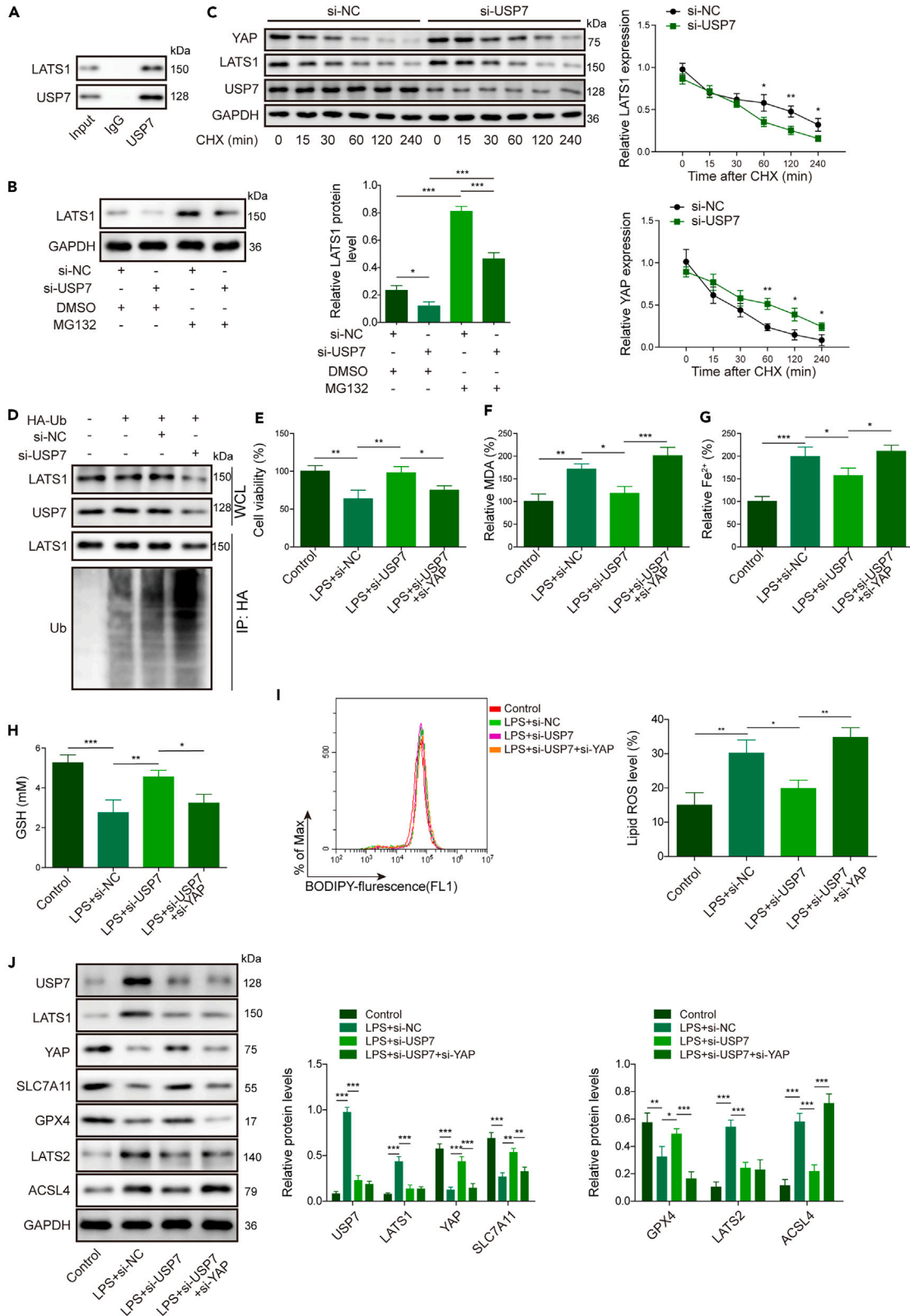
Figure 7. USP7 degrades YAP through deubiquitinating and stabilizing LATS1

(A) The hypothesized interaction between USP7 and LATS1 was tested by Co-IP assay.

(B) MLE-12 cells were transfected with si-USP7 and LATS1 expression was compared after MG132 treatment.

(C) MLE-12 cells were transfected with si-USP7, followed by CHX treatment. Western blot was performed to examine the degradation of LATS1 and YAP.

(D) Knockdown of USP7 deubiquitinates LATS1 *in vitro*.

(E) LPS-treated MLE-12 cells were transfected with LPS + si-NC, LPS + si-USP7, or LPS + si-USP7+si-YAP, and cell vitality was assessed by MTT assay.

(F) The lipid peroxide MDA expression level was compared among the indicated cells above.

(G) Cellular Fe^{2+} and (H) GSH changes were measured upon the specific treatments.

(I) Lipid ROS content was detected in cellular models.

(J) Protein expression of USP7, LATS1/2, YAP, GPX4, SLC7A11, and ACSL4 in the cells above was detected by western blot analysis. The experiment was repeated independently at least three times, and data were presented as mean $\pm$ standard deviation (S.D).*$p < 0.05$, **$p < 0.01$, ***$p < 0.001$ by Student's t test for C, and by one-way ANOVA test for B, E–J.

deubiquitinates and stabilizes LATS1/2. Notably, the inhibitory effect of YAP on ferroptosis was enhanced by knockdown of USP7 or LATS1 in our cellular ALI model. Another novel finding presented in this report is that YAP stimulated expression of GPX4 and SLC7A11 by regulating the association of TEAD4 on GPX4/SLC7A11 promoters. It is noteworthy that TGF-β1 successfully nullified the repression of ferroptosis which was mediated by YAP overexpression or the knockdown of LATS1 or USP7. Our results demonstrated that TGF-β1 is an important promoter of the ferroptosis process during ALI progression. TGF-β1 exerted its regulatory function by targeting USP7-LATS1-YAP-SLC7A11/GPX4 anti-oxidant response pathway. Although targeting TGF-β1 may be considered for the treatment of sepsis-induced lung injury, careful balance is required as both excessive inhibition and stimulation of TGF-β1 may have detrimental effects. Earlier research has demonstrated that both YAP and TAZ act as transcriptional coactivators in the regulation of ferroptosis.[39] Nonetheless, we have yet to conduct the necessary studies in the future to determine whether the aforementioned model is valid for TAZ, the paralog of YAP.

The research has aided in unraveling important information toward comprehending the pathogenesis of sepsis-secondary ALI pathogenesis. By elucidating the significant function of TGF-β1 in regulating ferroptosis and identifying the molecular interaction mechanisms involving TGF-β1, USP7, LATS1/2, YAP, GPX4, and SLC7A11, our findings could assist in developing innovative therapeutic approaches for the treatment of ALI.

Limitations of the study

Limitations of study are mainly reflected in the following aspects. Firstly, we did not knock down LATS2 to investigate the impact of USP7/LATS2/YAP axis on ferroptosis in depth; Secondly, that TGF-β1 regulates the impact of USP7/LATS1/2/YAP axis on ferroptosis was not validated in *in vivo* animal experiments; Thirdly, there is a lack of critical clinical data that cannot provide direct and effective strategies for treatment of ALI. Thus, more efforts are needed to further compensate for the shortcomings in clinical and *in vivo* experiments.

STAR★METHODS

Detailed methods are provided in the online version of this paper and include the following:

- KEY RESOURCES TABLE
- RESOURCE AVAILABILLITY
  - Lead contact
  - Materials availability
  - Data and code availability
- EXPERIMENTAL MODEL AND STUDY PARTICIPANT DETAILS
- METHOD DETAILS
  - Cell culture and LPS-Stimulation
  - Mouse sepsis model
  - Lung injury score calculation
  - Hematoxylin and eosin (H&E) staining
  - Plasmid synthesis and cell transfection
  - Cell viability assay (MTT assay)
  - Quantification of lipid reactive oxygen species (ROS)
  - Cellular glutathione (GSH) detection
  - Lipid peroxidation characterization by malondialdehyde (MDA) assay
  - Colorimetric detection of cellular iron ion
  - Protein preparation and western blot
  - Luciferase reporter assay
  - Chromatin immunoprecipitation (ChIP)-qPCR
  - Protein complex immunoprecipitation (Co-IP)
  - Deubiquitination detection and protein stability assay

● QUANTIFICATION AND STATISTICAL ANALYSIS

AUTHOR CONTRIBUTIONS

Guarantor of integrity of the entire study: H.L., J.Y., B.Z., and B.L.; study concepts: H.L., J.Y., B.Z., and B.L.; study design: H.L., J.Y., B.Z., and B.L.; definition of intellectual content: H.L. and J.Y.; literature research: L.S.; clinical studies: X.Q. and D.S.; experimental studies: J.S. and Z.T.; data acquisition: Q.Q. and G.F.; data analysis: H.L. and J.Y.; statistical analysis: H.L. and J.Y.; manuscript preparation: H.L., J.Y., B.Z., and B.L.

DECLARATION OF INTERESTS

The authors declare no competing interests.

REFERENCES

1. Cecconi, M., Evans, L., Levy, M., and Rhodes, A. (2018). Sepsis and septic shock. Lancet *392*, 75–87. https://doi.org/10.1016/S0140-6736(18)30696-2.

2. Butt, Y., Kurdowska, A., and Allen, T.C. (2016). Acute Lung Injury: A Clinical and Molecular Review. Arch. Pathol. Lab Med. *140*, 345–350. https://doi.org/10.5858/arpa.2015-0519-RA.

3. Rudd, K.E., Johnson, S.C., Agesa, K.M., Shackelford, K.A., Tsoi, D., Kievlan, D.R., Colombara, D.V., Ikuta, K.S., Kissoon, N., Finfer, S., et al. (2020). Global, regional, and national sepsis incidence and mortality, 1990-2017: analysis for the Global Burden of Disease Study. Lancet *395*, 200–211. https://doi.org/10.1016/S0140-6736(19)32989-7.

4. Varisco, B.M. (2011). The pharmacology of acute lung injury in sepsis. Adv. Pharmacol. Sci. *2011*, 254619. https://doi.org/10.1155/2011/254619.

5. Rubenfeld, G.D., Caldwell, E., Peabody, E., Weaver, J., Martin, D.P., Neff, M., Stern, E.J., and Hudson, L.D. (2005). Incidence and outcomes of acute lung injury. N. Engl. J. Med. *353*, 1685–1693. https://doi.org/10.1056/NEJMoa050333.

6. Kajarabille, N., and Latunde-Dada, G.O. (2019). Programmed Cell-Death by Ferroptosis: Antioxidants as Mitigators. Int. J. Mol. Sci. *20*, 4968. https://doi.org/10.3390/ijms20194968.

7. Doll, S., Proneth, B., Tyurina, Y.Y., Panzilius, E., Kobayashi, S., Ingold, I., Irmler, M., Beckers, J., Aichler, M., Walch, A., et al. (2017). ACSL4 dictates ferroptosis sensitivity by shaping cellular lipid composition. Nat. Chem. Biol. *13*, 91–98. https://doi.org/10.1038/nchembio.2239.

8. Dong, H., Qiang, Z., Chai, D., Peng, J., Xia, Y., Hu, R., and Jiang, H. (2020). Nrf2 inhibits ferroptosis and protects against acute lung injury due to intestinal ischemia reperfusion via regulating SLC7A11 and HO-1. Aging (Albany NY) *12*, 12943–12959. https://doi.org/10.18632/aging.103378.

9. Liu, P., Feng, Y., Li, H., Chen, X., Wang, G., Xu, S., Li, Y., and Zhao, L. (2020). Ferrostatin-1 alleviates lipopolysaccharide-induced acute lung injury via inhibiting ferroptosis. Cell. Mol. Biol. Lett. *25*, 10. https://doi.org/10.1186/s11658-020-00205-0.

10. Sun, T., and Chi, J.T. (2021). Regulation of ferroptosis in cancer cells by YAP/TAZ and Hippo pathways: The therapeutic implications. Genes Dis. *8*, 241–249. https://doi.org/10.1016/j.gendis.2020.05.004.

11. Chen, L., Chan, S.W., Zhang, X., Walsh, M., Lim, C.J., Hong, W., and Song, H. (2010). Structural basis of YAP recognition by TEAD4 in the hippo pathway. Genes Dev. *24*, 290–300. https://doi.org/10.1101/gad.1865310.

12. Chen, M., Huang, B., Zhu, L., Chen, K., Liu, M., and Zhong, C. (2020). Structural and Functional Overview of TEAD4 in Cancer Biology. OncoTargets Ther. *13*, 9865–9874. https://doi.org/10.2147/OTT.S266649.

13. Gao, R., Kalathur, R.K.R., Coto-Llerena, M., Ercan, C., Buechel, D., Shuang, S., Piscuoglio, S., Dill, M.T., Camargo, F.D., Christofori, G., and Tang, F. (2021). YAP/TAZ and ATF4 drive resistance to Sorafenib in hepatocellular carcinoma by preventing ferroptosis. EMBO Mol. Med. *13*, e14351. https://doi.org/10.15252/emmm.202114351.

14. Yang, W.H., Lin, C.C., Wu, J., Chao, P.Y., Chen, K., Chen, P.H., and Chi, J.T. (2021). The Hippo Pathway Effector YAP Promotes Ferroptosis via the E3 Ligase SKP2. Mol. Cancer Res. *19*, 1005–1014. https://doi.org/10.1158/1541-7786.MCR-20-0534.

15. Liu, L.Y., Shan, X.Q., Zhang, F.K., Fan, X.F., Fan, J.M., Wang, Y.Y., Liu, S.F., Mao, S.Z., and Gong, Y.S. (2020). YAP activity protects against endotoxemic acute lung injury by activating multiple mechanisms. Int. J. Mol. Med. *46*, 2235–2250. https://doi.org/10.3892/ijmm.2020.4759.

16. Ursini, F., and Maiorino, M. (2020). Lipid peroxidation and ferroptosis: The role of GSH and GPx4. Free Radic. Biol. Med. *152*, 175–185. https://doi.org/10.1016/j.freeradbiomed.2020.02.027.

17. Park, T.J., Park, J.H., Lee, G.S., Lee, J.Y., Shin, J.H., Kim, M.W., Kim, Y.S., Kim, J.Y., Oh, K.J., Han, B.S., et al. (2019). Quantitative proteomic analyses reveal that GPX4 downregulation during myocardial infarction contributes to ferroptosis in cardiomyocytes. Cell Death Dis. *10*, 835. https://doi.org/10.1038/s41419-019-2061-8.

18. Yang, W.S., SriRamaratnam, R., Welsch, M.E., Shimada, K., Skouta, R., Viswanathan, V.S., Cheah, J.H., Clemons, P.A., Shamji, A.F., Clish, C.B., et al. (2014). Regulation of ferroptotic cancer cell death by GPX4. Cell *156*, 317–331. https://doi.org/10.1016/j.cell.2013.12.010.

19. Ye, Y., Chen, A., Li, L., Liang, Q., Wang, S., Dong, Q., Fu, M., Lan, Z., Li, Y., Liu, X., et al. (2022). Repression of the antiporter SLC7A11/glutathione/glutathione peroxidase 4 axis drives ferroptosis of vascular smooth muscle cells to facilitate vascular calcification. Kidney Int. *102*, 1259–1275. https://doi.org/10.1016/j.kint.2022.07.034.

20. Wang, J., Li, H.Y., and Su, Z.B. (2020). Stabilization of the histone acetyltransferase Tip60 by deubiquitinating enzyme USP7 stimulates the release of pro-inflammatory mediators in acute lung injury. J. Mol. Med. *98*, 907–921. https://doi.org/10.1007/s00109-020-01910-1.

21. Dong, B., Ding, C., Xiang, H., Zheng, J., Li, X., Xue, W., and Li, Y. (2022). USP7 accelerates FMR1-mediated ferroptosis by facilitating TBK1 ubiquitination and DNMT1 deubiquitination after renal ischemia-reperfusion injury. Inflamm. Res. *71*, 1519–1533. https://doi.org/10.1007/s00011-022-01648-1.

22. Tang, L.J., Zhou, Y.J., Xiong, X.M., Li, N.S., Zhang, J.J., Luo, X.J., and Peng, J. (2021). Ubiquitin-specific protease 7 promotes ferroptosis via activation of the p53/TfR1

pathway in the rat hearts after ischemia/reperfusion. Free Radic. Biol. Med. *162*, 339–352. https://doi.org/10.1016/j.freeradbiomed.2020.10.307.

23. Pittet, J.F., Griffiths, M.J., Geiser, T., Kaminski, N., Dalton, S.L., Huang, X., Brown, L.A., Gotwals, P.J., Koteliansky, V.E., Matthay, M.A., and Sheppard, D. (2001). TGF-beta is a critical mediator of acute lung injury. J. Clin. Invest. *107*, 1537–1544. https://doi.org/10.1172/JCI11963.

24. de Pablo, R., Monserrat, J., Reyes, E., Díaz, D., Rodríguez-Zapata, M., la Hera, A.d., Prieto, A., and Alvarez-Mon, M. (2012). Sepsis-induced acute respiratory distress syndrome with fatal outcome is associated to increased serum transforming growth factor beta-1 levels. Eur. J. Intern. Med. *23*, 358–362. https://doi.org/10.1016/j.ejim.2011.10.001.

25. Liu, R.M., and Desai, L.P. (2015). Reciprocal regulation of TGF-beta and reactive oxygen species: A perverse cycle for fibrosis. Redox Biol. *6*, 565–577. https://doi.org/10.1016/j.redox.2015.09.009.

26. Han, C., Liu, Y., Dai, R., Ismail, N., Su, W., and Li, B. (2020). Ferroptosis and Its Potential Role in Human Diseases. Front. Pharmacol. *11*, 239. https://doi.org/10.3389/fphar.2020.00239.

27. Zhao, Y., Li, Y., Zhang, R., Wang, F., Wang, T., and Jiao, Y. (2020). The Role of Erastin in Ferroptosis and Its Prospects in Cancer Therapy. OncoTargets Ther. *13*, 5429–5441. https://doi.org/10.2147/OTT.S254995.

28. Delvaux, M., Hagué, P., Craciun, L., Wozniak, A., Demetter, P., Schöffski, P., Erneux, C., and Vanderwinden, J.M. (2022). Ferroptosis Induction and YAP Inhibition as New Therapeutic Targets in Gastrointestinal Stromal Tumors (GISTs). Cancers *14*, 5050. https://doi.org/10.3390/cancers14205050.

29. Sevransky, J.E., Martin, G.S., Shanholtz, C., Mendez-Tellez, P.A., Pronovost, P., Brower, R., and Needham, D.M. (2009). Mortality in sepsis versus non-sepsis induced acute lung injury. Crit. Care *13*, R150. https://doi.org/10.1186/cc8048.

30. Dixon, S.J., Lemberg, K.M., Lamprecht, M.R., Skouta, R., Zaitsev, E.M., Gleason, C.E., Patel, D.N., Bauer, A.J., Cantley, A.M., Yang, W.S., et al. (2012). Ferroptosis: an iron-dependent form of nonapoptotic cell death. Cell *149*, 1060–1072. https://doi.org/10.1016/j.cell.2012.03.042.

31. Kim, D.H., Kim, W.D., Kim, S.K., Moon, D.H., and Lee, S.J. (2020). TGF-beta1-mediated repression of SLC7A11 drives vulnerability to GPX4 inhibition in hepatocellular carcinoma cells. Cell Death Dis. *11*, 406. https://doi.org/10.1038/s41419-020-2618-6.

32. Li, X., Duan, L., Yuan, S., Zhuang, X., Qiao, T., and He, J. (2019). Ferroptosis inhibitor alleviates Radiation-induced lung fibrosis (RILF) via down-regulation of TGF-beta1. J. Inflamm. *16*, 11. https://doi.org/10.1186/s12950-019-0216-0.

33. Kim, S., Kang, S.W., Joo, J., Han, S.H., Shin, H., Nam, B.Y., Park, J., Yoo, T.H., Kim, G., Lee, P., and Park, J.T. (2021). Characterization of ferroptosis in kidney tubular cell death under diabetic conditions. Cell Death Dis. *12*, 160. https://doi.org/10.1038/s41419-021-03452-x.

34. Deng, J.C., and Standiford, T.J. (2011). Growth factors and cytokines in acute lung injury. Compr. Physiol. *1*, 81–104. https://doi.org/10.1002/cphy.c090011.

35. Qian, M., Lou, Y., Wang, Y., Zhang, M., Jiang, Q., Mo, Y., Han, K., Jin, S., Dai, Q., Yu, Y., et al. (2018). PICK1 deficiency exacerbates sepsis-associated acute lung injury and impairs glutathione synthesis via reduction of xCT. Free Radic. Biol. Med. *118*, 23–34. https://doi.org/10.1016/j.freeradbiomed.2018.02.028.

36. Zhang, J., Smolen, G.A., and Haber, D.A. (2008). Negative regulation of YAP by LATS1 underscores evolutionary conservation of the Drosophila Hippo pathway. Cancer Res. *68*, 2789–2794. https://doi.org/10.1158/0008-5472.CAN-07-6205.

37. Sun, X., Ding, Y., Zhan, M., Li, Y., Gao, D., Wang, G., Gao, Y., Li, Y., Wu, S., Lu, L., et al. (2019). Usp7 regulates Hippo pathway through deubiquitinating the transcriptional coactivator Yorkie. Nat. Commun. *10*, 411. https://doi.org/10.1038/s41467-019-08334-7.

38. Li, J., Dai, Y., Ge, H., Guo, S., Zhang, W., Wang, Y., Liu, L., Cheng, J., and Jiang, H. (2022). The deubiquitinase USP7 promotes HNSCC progression via deubiquitinating and stabilizing TAZ. Cell Death Dis. *13*, 677. https://doi.org/10.1038/s41419-022-05113-z.

39. Lo Sardo, F., Canu, V., Maugeri-Saccà, M., Strano, S., and Blandino, G. (2022). YAP and TAZ: Monocorial and bicorial transcriptional co-activators in human cancers. Biochim. Biophys. Acta Rev. Canc *1877*, 188756. https://doi.org/10.1016/j.bbcan.2022.188756.

STAR★METHODS

KEY RESOURCES TABLE

REAGENT or RESOURCE	SOURCE	IDENTIFIER
Antibodies		
USP7	Abcam	Cat# ab109109; RRID:AB_10888297
YAP	Abcam	Cat# ab205270; RRID:AB_2813833
LATS1	Abcam	Cat# ab85893; RRID:AB_1925171
LATS2	Abcam	Cat# ab54073; RRID:AB_2133372
GPX4	Abcam	Cat# ab125066; RRID:AB_1097390
SLC7A11	Abcam	Cat# ab175186; RRID:AB_2722749
ACSL4	Abcam	Cat# ab155282; RRID:AB_271402
GAPDH	Abcam	Cat# ab8245; RRID:AB_2107448
IgG	Abcam	Cat# ab109489; RRID:AB_10863040
HRP secondary antibody	Abcam	Cat# ab205718; RRID:AB_2819160
TEAD4	Abcam	Cat# ab58310; RRID:AB_945789
Ubiquitin	Abcam	Cat# ab140601; RRID:AB_2783797
Chemicals, peptides, and recombinant proteins		
TGF-β1	Sigma	Cat# T7039
Fe-citrate (III)	Sigma	Cat# 1185-57-5
Ferrostatin-1	MedChemExpress	Cat# HY-100579
Lipopolysaccharides	MedChemExpress	Cat# HY-D1056
Erastin	MedChemExpress	Cat# HY-15763
Cycloheximide	Merck	Cat# 66-81-9
BODIPY™ 581/591 C11	Invitrogen™	Cat# D3861
RNase A	Thermo Scientific	Cat# EN0531
proteinase K	Thermo Scientific	Cat# EO0491
PMSF	Sigma	Cat# 329-98-6
Aprotinin	Sigma	Cat# 02-0781-00
DNase I	Sigma	Cat# 3750-OP
Protein A/G beads	Sigma	Cat# 88802
DMSO	Merck	Cat# D2650
MG132	CST	Cat #2194
cocktail	Sigma	Cat #539132
Lipofectamine 2000 reagent	Invitrogen	Cat# 4476093001
ECL	Beyotime	Cat# P0018S
Critical commercial assays		
MDA Assay Kit (Colorimetric)	Abcam	Cat# ab118970
MTT Cell Viability Assay Kit	ThermoFisher	Cat# V13154
GSH Detection Assay Kit	Abcam	Cat# ab112132
Iron Assay Kit	Abcam	Cat# ab83366
Dual-Luciferase Reporter Assay System	Thermo Scientific™	Cat# ab16186
ChIP Assay Kit	Pierce	Cat# 26159

Continued

REAGENT or RESOURCE	SOURCE	IDENTIFIER
Deposited data		
JASPAR	This paper	Figures 6B/6G; https://jaspar.elixir.no/
Ubibrowser	This paper	Figure 5A; http://ubibrowser.bio-it.cn/ubibrowser_v3/
Experimental models: Cell lines		
MLE-12	ATCC	RRID: Cat# CRL-2110
Experimental models: Organisms/strains		
Male C57BL/6J	Shanghai SLAC Laboratory Animal Co., Ltd	N/A
Oligonucleotides		
siRNA targeting sequence: USP7: 5′- GCCACTTGTTCTTCCACAAGG-3′	This paper	N/A
siRNA targeting sequence: LATS1: 5′- CCACCCAAATTTGGCACACATCATA-3′	This paper	N/A
siRNA targeting sequence: YAP: 5′- CGGTTGAAACAACAGGAATTA-3′	This paper	N/A
BS1(ChIP) for GPX4 promoter: AGGCTCTGTCCA	This paper	N/A
BS2(ChIP) for GPX4 promoter: CTGAGTCAC	This paper	N/A
BS1(ChIP) for SLC7A11 promoter: CAGATAAGG	This paper	N/A
BS2(ChIP) for SLC7A11 promoter: AGAGTAAACA	This paper	N/A
Recombinant DNA		
Plasmid: pMIR-report luciferase	YouBio	RRID: Cat# VT1399
Plasmid: pcDNA3.1	YouBio	RRID: Cat# VT1001
Software and algorithms		
ImageJ	Schneider et al.[7]	https://imagej.nih.gov/ij/
EnSpire-Multimode Plate-Reader	PerkinElmer	N/A
Leica microscope	DMIRB	N/A

RESOURCE AVAILABILLITY

Lead contact

Further information and request for resources and reagents should be directed to and will be fulfilled by the lead contact, Bing Lu (tczyyLb@163.com).

Materials availability

This study did not generate new unique reagents.

Data and code availability

- All data reported in this paper will be shared by the lead contact upon request.
- This paper does not report original code.
- Any additional information required to reanalyze the data reported in this paper is available from the lead contact upon request.

EXPERIMENTAL MODEL AND STUDY PARTICIPANT DETAILS

Male C57BL/6J mice of the wild type, aged 6–8 weeks, were procured from Shanghai SLAC Laboratory Animal Co., Ltd. All the animal experimental procedures were performed in accordance with the Institutional Animal Care and Use Committee of the Taicang TCM Hospital, affiliated with Nanjing University of Chinese Medicine and the study were approved by the Taicang TCM Hospital, Affliated to Nanjing University of Chinese Medicine. They were housed in an air-conditioned animal room (23°C, 55% ± 5%, 12 h light–dark cycle) with free access to standard laboratory chow and clean water. To induce acute lung injury (ALI) in the animal sepsis model, the cecal ligation and puncture (CLP) procedure was performed. The study comprised six groups of mice, randomly divided: CLP ($n = 8$), CLP + Fe ($n = 8$), CLP + Fer-1 ($n = 8$), CLP + TGF-β1 ($n = 8$), CLP + TGF-β1+Fer-1 ($n = 8$), and sham ($n = 8$). The mice were anesthetized with an intraperitoneal injection of a ketamine-xylazine mixture (100 and 5 mg/kg body weight, respectively). A 1-cm longitudinal incision was made in the lower abdomen, and the peritoneal cavity was further cut to expose the cecum. The cecum was then ligated below the ileocecal valve and perforated with a 21- gauge needle. After removing the needle, a small amount of feces was carefully extruded. Finally, the exteriorized cecum was replaced and the abdominal cavity was closed using a sterile 4-0 surgical suture. The sham-operated group underwent a skin-incision procedure identical to that of the experimental group, but the cecum was identified without ligation or puncture. On day 7, the ferroptosis process was promoted by intraperitoneal injection of Fe-citrate (III)/Fe (15 mg/kg, Sigma) and inhibited by administration of ferrostatin-1 (Fer-1, 1.5 mg/kg/i.p. injection, Sigma) once per day for two weeks. Recombinant TGF-β1 (10 mg/kg, Invitrogen) was injected intraperitoneally twice daily for three days. The survival rate was analyzed every 12 h. All animals were received 1 mL of saline for fluid resuscitation and were euthanized 4, 8, or 24 h after the CLP operation for subsequent experimental analysis. Histopathological changes in lung samples were examined using H&E staining. The expression of USP7, LATS1/2, YAP, GPX4, SLC7A11, and ACSL4 was evaluated using Western blot analysis. The Wet/Dry ratio of lung weight was measured as an index of pulmonary edema. The right lower lungs were dissected from each mouse group 24 h after the CLP operation and weighed immediately as wet weight. The lung tissues were then dehydrated in an oven at 70°C for 48 h, and the dry weight was measured to calculate the Wet/Dry ratio.

METHOD DETAILS

Cell culture and LPS-Stimulation

Mouse lung epithelial cells MLE-12 (CVCL_3751), a mouse lung epithelial cell line, were obtained from the ATCC (CRL-2110). Cells were revived, cultured in Ham's F-12K (Kaighn's) Medium (Thermo Fisher Scientific, Waltham MA) containing 10% fetal bovine serum (FBS, Gibco, CA, USA), 1% penicillin (Invitrogen, CA, USA) and streptomycin (Invitrogen, CA, USA), and maintained at 37°C (5% CO_2). To establish an *in vitro* septic model, MLE-12 cells were stimulated with LPS (5 μg/mL) for 24 h (Figure S1). Ferroptosis was induced by incubating the MLE-12 cells with increasing concentrations of erastin (0, 2.5, 5, 10, 20, 40 μM, MCE, HY-15763) for 24 h. 5 μM ferrostatin-1 (Fer-1, MCE, HY-100579) was added to inhibit the cellular ferroptosis. Biological effect of TGF-β1 during ferroptosis was tested by adding recombinant human TGF-β1 (Sigma-Aldrich, T7039) to the cells to a final concentration of 5 ng/mL.

Mouse sepsis model

Wild type male C57BL/6J mice (male, 6–8 weeks old, $n = 6$ per group) were purchased from Shanghai SLAC Laboratory Animal Co., Ltd and housed in an air-conditioned animal room (23°C, 55% ± 5%, 12 h light–dark cycle) with free access to standard laboratory chow and clean water. All the animal experimental procedures were approved by the Taicang TCM Hospital, Affliated to Nanjing University of Chinese Medicine and performed in accordance with the Institutional Animal Care and Use Committee of the Taicang TCM Hospital, Affliated to Nanjing University of Chinese Medicine. Cecal ligation and puncture (CLP) procedure was performed to induce acute lung injury (ALI) in the animal sepsis model. Mice were randomly divided to six groups throughout the study: CLP ($n = 8$), CLP + Fe ($n = 8$), CLP + Fer-1 ($n = 8$), CLP + TGF-β1 ($n = 8$), CLP + TGF-β1+Fer-1 ($n = 8$), and sham ($n = 8$). Briefly, mice were anesthetized with intraperitoneal injection of ketamine-xylazine mixture (100 and 5 mg/kg body weight, respectively), and 1-cm longitudinal incision was made at the lower abdomen and the cecum was exposed by further cutting the incision into the peritoneal cavity. Next, the cecum was ligated below the ileocecal valve and perforated with a 21- Gauge needle. After the needle was removed, a small amount of feces was carefully extruded. Finally, the exteriorized cecum was placed back and the abdominal cavity was closed using a sterile 4-0 surgical suture. Sham-operated group underwent skin-incision procedure identically and the cecum was identified without ligation or puncture. At day 7 ferroptosis process was promoted by intraperitoneal injection of Fe-citrate (III)/Fe (15 mg/kg, Sigma) and inhibited by ferrostatin-1 administration (Fer-1, 1.5 mg/kg/i.p. injection, Sigma) once per day for two weeks. Recombinant TGF-β1 (10 mg/kg, Invitrogen) was i.p. injected twice daily for three days. Survival rate was analyzed every 12 h. All animals were injected with 1 mL saline for fluid resuscitation and euthanized 4, 8, or 24 h post-CLP operation for subsequent experimental analysis. Histopathological changes in lung samples were examined by H&E staining. Expression of USP7, LATS1/2, YAP, GPX4, SLC7A11, and ACSL4 was evaluated by Western blot analysis. The Wet/Dry ratio of lung weight was measured as an index of pulmonary edema. 24 h after CLP operation, right lower lungs were dissected from each mouse group and immediately weighed as wet weight. Next, the lung tissues were dehydrated in an oven at 70°C for 48 h and dry weight was measured the Wet/Dry ratio.

Lung injury score calculation

Lung injury prediction scores were calculated by a blinded researcher using the previously described criteria, including neutrophil in the alveolar space, neutrophils in the interstitial space, hyaline membrane, proteinaceous debris filling the airspace and alveolar septal thickening. The values above were summed up and final score was derived by dividing the number of fields.

Hematoxylin and eosin (H&E) staining

Mice were sacrificed and left lungs were collected. Lung tissues were fixed with 4% paraformaldehyde for 24 h, followed by paraffin wax immersion and embedding. Samples were then cut into 4-mm coronal sections and mounted on positively charged glass slides for H&E staining. Briefly, the sections were processed three times with xylene for deparaffinization and rehydrated with decreasing concentration of ethanol. Next, sections were incubated with hematoxylin for 3 min at room temperature and quickly rinsed with 1% acid ethanol to sharpen the eosin staining. After washing under tap water, the sections were incubated with 0.5% eosin for 1 min and dehydrated using increasing concentrations of ethanol. Finally, sections were processed three times with xylene, and one drop of Permount (VWR, South Plainfield, NJ, USA) was dispensed to the slide before sealing with coverslips. Slides were dried overnight and images were acquired under a Leica microscope (DMIRB, Germany).

Plasmid synthesis and cell transfection

Small interfering RNAs (siRNA) against USP7, YAP and LATS1 (si-USP7, si-YAP and si-LATS1) were designed and synthesized by GenePharma (Shanghai, China). The sequences for si-USP7, si-YAP and si-LATS1 were provided in Table S1. Gene sequences encoding YAP as well as the siRNAs above were subcloned into pcDNA3.1 vector respectively. MLE-12 cells were plated on a 6-well plate and grown to 80% confluency, followed by transfection with pcDNA3.1-YAP, pcDNA3.1-si-USP7, pcDNA3.1-si-YAP or pcDNA3.1-si-LATS1 using Lipofectamine 2000 (Invitrogen). Cells transfected with empty vector pcDNA-NC were used as negative control. 48 h after transfection cells were harvested and washed with PBS for subsequent experiments.

Cell viability assay (MTT assay)

Cellular apoptosis was detected by MTT method using the CyQUANT MTT Cell Viability Assay Kit (ThermoFisher, V13154) according to the user's guidelines. Briefly, cells were transfected on a 96-well plate and supplemented with erastin at concentration of 0, 2.5, 5, 10, 20 or 40 μM. 10 μL of 12-mM MTT stock reagent (3-(4, 5-dimethylthiazol-2-yl)-2, 5-diphenyltetrazoliumbromide) was added to each well and the mixture was incubated at 37°C for 4 h. Next, 100 μL of SDS-HCL was added to each well, followed by incubation at 37°C for 10 h. Finally, samples were well mixed by pipetting up and down, and the absorbance at 490 nm was recorded at EnSpire-Multimode Plate-Reader (PerkinElmer).

Quantification of lipid reactive oxygen species (ROS)

Lipid ROS content in cellular and animal models were determined using BODIPY-based fluorescent probes. Precisely, samples of cells or tissues were washed and incubated with C11 BODIPY 581/591 (Thermo Fisher Scientific) at a final concentration of 10 μM concentration for 30 min. Afterward, the reaction was centrifuged at 400 g and washed twice with PBS. Finally, the fluorescent signals were measured through flow cytometry with excitation at 488 nm and 581 nm wavelengths.

Cellular glutathione (GSH) detection

Redox and detoxification status in cells and tissue samples was evaluated by measuring the glutathione level using Intracellular glutathione (GSH) Detection Assay Kit (Abcam, UK), according to the manufacturer's protocol. Briefly, 1 mL of MLE-12 cells at cell density of 1×10^6 cells/mL were incubated with 5 μL of 200× Thiol Green Dye for 20 min at 37°C. The mixture was centrifuged at 500 g for 10 min and cells were resuspended in 1 mL of new complete F-12K Medium. Finally, cells were profiled on a flow cytometer and fluorescence intensity was recorded at Ex/Em = 490/525 nm.

Lipid peroxidation characterization by malondialdehyde (MDA) assay

Lipid peroxidation in cells and tissue samples was characterized by running an MDA assay using Lipid Peroxidation (MDA) Assay Kit (Colorimetric) (Abcam, UK, ab118970). Briefly, 200 μL of MDA standards at 0, 4, 8, 12, 16 and 20 nM were prepared for colorimetric detection, according to the user's guide. 1×10^6 cells were homogenized in 300 μL of MDA lysis buffer supplemented with 3 μL of BHT. Cell debris was removed by centrifuging the samples at 13,000 × g for 10 min, and MDA-TBAadduct was formed by incubating the centrifuge supernatant with 600 μL thiobarbituric acid (TBA) at 95°C for 60 min. Finally, 200 μL of the reaction mixture was transferred to a 96-well plate and absorbance at 532 nm at the Plate-Reader.

Colorimetric detection of cellular iron ion

Cellular ferrous (Fe^{2+}) and ferric ion (Fe^{3+}) that play important roles in redox hemostasis was detected by Iron Assay Kit (Abcam, UK, ab83366). Briefly, iron standards at 0, 2, 4, 6, 8 and 10 nM were prepared by diluting the 1 mM Iron standard solution with water. 2×10^6 cells were homogenized in 250 μL ice-cold Iron Assay Buffer and cell debris was removed by centrifuging the samples at 13,000 × g for 10 min. Next, 1–50 μL of centrifuge supernatant and 5 μL Iron Assay Buffer was added in a 96-well plate. Final volume was adjusted to 100 μL/well using the Iron Assay Buffer, and the reaction mixture was incubated at 37°C for 30 min. Finally, 100 μL of Iron probe was added to the wells containing the Iron Standards or cell sample and incubated at 37°C for 60 min. Absorbance at 532 nm was measured at the Plate-Reader.

Protein preparation and western blot

MLE-12 cells and tissue samples were homogenized in ice-cold RIPA lysis buffer supplemented with protease inhibitor cocktail (Sigma, USA). Cell debris was removed by centrifuging at 13,000 × g for 15 min 50 μg of protein homogenate was separated on a 12% SDS-PAGE and transferred to Immobilon PVDF membrane (Sigma). GAPDH was loaded as a positive control. Membrane was blocked with 5% non-fat milk to prevent non-specific bindings. Next, primary antibodies against USP7 (1:3000 dilution, Abcam, ab109109), YAP (1:1000 dilution, Abcam, ab205270), LATS1 (1:1000 dilution, Abcam, ab243656), LATS2 (1:1000 dilution, Abcam, ab243657), SLC7A11 (1:3000, Abcam, ab175186), GPX4 (1:1000 dilution, Abcam, ab125066), ACSL4 (1:10000 dilution, Abcam, ab155282), or GAPDH (1:1000 dilution, Abcam, ab8245), which were included in Table S2, were added to the membranes, and incubated at 4°C overnight. After three washes in 100 μM PBST, membranes were incubated with goat anti-rabbit HRP secondary antibodies (1:3000 dilutions, Abcam, ab205718) for 1 h at room temperature. Protein bands were visualized by using the ECL chemiluminescent detection system (Amersham Pharmacia Biotech, NJ).

Luciferase reporter assay

JASPAR database was accessed and putative binding sites between TEAD4 and GPX4/SLC7A11 promoters were computed. The promoter of GPX4 wild-type (GPX4-WT) and SLC7A11 wild-type (SLC7A11-WT) that contain TEAD4 binding sequence were inserted into the luciferase reporter vector pMIR-report. The constructs GPX4-MUT1, GPX4-MUT2, GPX4-MUT1&2, SLC7A11-MUT1, SLC7A11-MUT2 and SLC7A11-MUT1&2 carrying the mutated TEAD4-binding sites was generated using a QuikChange site-directed mutagenesis kit (Stratagene, La Jolla, CA, USA). MLE-12 cells were seeded on a 96-well plate and grown to 60% confluence. To detect the binding between TEAD4 and GPX4, cells were co-transfected with 25 ng GPX4-WT Luciferase reporter, 25 ng GPX4-MUT1 Luciferase reporter, 25 ng GPX4-MUT2 Luciferase reporter, 25 ng GPX4-MUT1&2 Luciferase reporter, pcDNA-3.1-TEAD4 or the empty pcDNA-3.1 vector (EV) using Lipofectamine 2000 (Invitrogen, USA). Cells were transfected with YAP plasmids at the concentration of 0 or 100 ng/mL and harvested 24 h after transfection. To detect the binding between TEAD4 and SLC7A11, cells were co-transfected with 25 ng SLC7A11-WT Luciferase reporter, 25 ng SLC7A11-MUT1 Luciferase reporter, 25 ng SLC7A11-MUT2 Luciferase reporter, 25 ng SLC7A11-MUT1&2 Luciferase reporter, pcDNA-3.1-TEAD4 or the empty pcDNA-3.1 vector (EV). Cells were transfected with YAP plasmids at the concentration of 0 or 100 ng/mL, and harvested 24 h after transfection Reporter assays were performed using Dual-Luciferase Reporter Assay System (Promega, Madison, WI, USA), according to the manufacturer's instructions. Both Firefly and Renilla luciferase activities were simultaneously detected.

Chromatin immunoprecipitation (ChIP)-qPCR

Relative enrichment of TEAD4 at GPX4 and SLC7A11 promoters were quantified by ChIP-qPCR method. Briefly, MLE-12 cells were transfected with YAP plasmids at the concentrations of 0, 20, 50 or 100 ng/mL. After 48 h of incubation, chromatin-protein chemical links were formed by incubating MLE-12 cells with formaldehyde at a final concentration of 1% for 10 min. Cells were lysed in ice-cold ChIP lysis buffer and DNA fragments of 500 bp were generated by 30 min sonication. Cell debris was removed by centrifuging at 13,000 × g for 15 min. DNA sizes were determined by loading 10 μL of the supernatant on agarose gel and DNA concentration was estimated by measuring the 260 nm absorbance. Chromatin-protein complexes were immunoprecipitated with the TEAD4-specific primary antibody (1:1000 dilution, Abcam, ab155244), or the control IgG for 1 h at 4°C. Equal volume of Protein A and Protein G beads were mixed and non-specific DNA-binding sites were blocked by adding single-stranded herring sperm DNA to the agarose beads. Immunoprecipitated samples were incubated with 60 μL of Protein A/G beads (Thermo Scientific, 88802) at 4°C overnight. Finally, samples above were washed with low salt and high salt wash buffer and DNA was eluted using 120 μL elution buffer. After treatments with 2 μL of RNase A (10 mg/mL, Thermo Scientific, EN0531) and 2 μL of proteinase K (20 mg/mL, Thermo Scientific, EO0491), DNA was purified for subsequent qRT-PCR assay.

Protein complex immunoprecipitation (Co-IP)

The physiologically relevant interaction between USP7 and LATS1 and the hypothesized complex formation was identified by Co-IP technique. Briefly, MLE-12 cells were trypsinized and washed three times with ice-cold PBS. Cells were then resuspended in ice-cold RIPA buffer supplemented with 50 μg/mL PMSF (Sigma), 1 μg/mL aprotinin (Sigma) and 20 mM DNase I (Sigma). Cell debris was removed by centrifuging at 13,000 × g for 15 min and supernatant was collected. 1 μg antibody against USP7 (1:3000 dilution, Abcam, ab109109) or LATS1 (1:1000 dilution, Abcam, ab243656) was added to 100 μL clarified cell lysate for overnight incubation at 4°C. Meanwhile, Protein A/G beads (Sigma) were washed twice with PBS and 100 μL of 50% Protein A/G agarose working solution was added to 1 mL sample solution. After 4 h incubation at 4°C, the mixture was centrifuged and non-specific binding was removed by washing complex-bound beads three times with washing buffer. Protein was eluted using 50 μL of 0.2 M glycine, pH 2.5 and neutralized using 50 μL of Tris, pH 8.0. Samples were loaded on SDS-PAGE and checked by Western blot.

Deubiquitination detection and protein stability assay

To address the deubiquitination and stabilization of LATS1 by USP7, MLE-12 cells were transfected with si-USP7 for knockdown. Prior to deubiquitination analysis, cells were incubated with the protein translation inhibitor cycloheximide at final concentration of 50 μg/mL (CHX, Merck, 66-81-9), proteasome blocker MG132 (Cell Signaling, #2194) or DMSO (Merck, D2650). Remaining ubiquitinated LATS1 was characterized using anti-Ubiquitin (1:1000 dilution, Abcam, ab140601) by Western blot. Degradation level of USP7 and LATS1 was monitored on Western Blot using antibodies against USP7 (1:3000 dilution, Abcam, ab109109) or LATS1 (1:1000 dilution, Abcam, ab243656).

QUANTIFICATION AND STATISTICAL ANALYSIS

All the experiments have been repeated at least three times. Data are expressed as the mean $\pm$ standard deviation (SD) and were analyzed using the GraphPad Prism 5.0 software (GraphPad Inc., San Diego, CA, USA). Survival probability was estimated by Kaplan-Meier curve and differences were compared among the sham, CLP, CLP + Fer, CLP + Fe and CLP + TGF-β1 groups. Statistical analysis was performed using the Student's t test or one-way ANOVA test. $p < 0.05$ was considered significant. *, $p < 0.05$, **, $p < 0.01$, ***, $p < 0.001$.